

Design and Fabrication of a Modular Multi-Material 3D Printer

by

Justin Lan

S.B. Mechanical Engineering

Massachusetts Institute of Technology, 2011

Submitted to the Department of Mechanical Engineering
in partial fulfillment of the requirements for the degree of

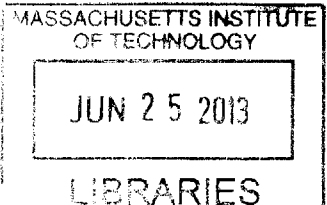
Master of Science in Mechanical Engineering

at the

MASSACHUSETTS INSTITUTE OF TECHNOLOGY

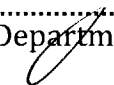
June 2013

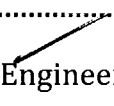
ARCHIVES



LIBRARIES

© Massachusetts Institute of Technology 2013. All rights reserved.

Author

Department of Mechanical Engineering
April 30, 2013

Certified by

Wojciech Matusik
Associate Professor of Electrical Engineering and Computer Science
Thesis Supervisor

Certified by

John Leonard
Professor of Mechanical Engineering
Mechanical Engineering Faculty Reader

Accepted by

David E. Hardt
Ralph E. and Eloise F. Cross Professor of Mechanical Engineering
Chairman, Department Committee on Graduate Students

Design and Fabrication of a Modular Multi-Material 3D Printer

by

Justin Lan

Submitted to the Department of Mechanical Engineering
on April 30, 2013, in partial fulfillment of the
requirements for the degree of
Master of Science in Mechanical Engineering

ABSTRACT

This thesis presents 3DP-0, a modular, multi-material 3D printer. Currently, 3D printers available on the market are typically expensive and difficult to develop. In addition, the simultaneous use of multiple materials in 3D printing has not been extensively explored. The printer presented in this thesis was developed to address these shortcomings. The printer features a low-cost high-performance design largely using commercial off-the-shelf parts. Inkjet print heads from commercial desktop printers allow the use of multiple materials within a single print. In addition, the modular and open design of the printer allows the independent and continuing development of print heads and print materials. Testing has shown the system to be capable of producing objects with fine features, including 500 μm -wide cubes containing multiple materials separated within a core.

Thesis Supervisor: Wojciech Matusik

Title: Associate Professor of Electrical Engineering and Computer Science

Mechanical Engineering Faculty Reader: John Leonard

Title: Professor of Mechanical Engineering

Acknowledgements

I would like to thank Professor Wojciech Matusik for giving me the opportunity to work on this exciting and engaging project. I would also like to extend my thanks to the members of the Computer Graphics Group, both for their technical support on the project and for being a fantastic community to be a part of these past two years.

I would also like to thank Ron Wiken of the CSAIL machine shop. I made most of the components used on the project in the CSAIL shop, and Ron was always there to provide help when I needed it.

Finally, I would like to thank my friends and family for their support during my time here at MIT. Thanks for helping me to keep things in perspective.

Contents

1	Introduction	6
2	Background	7
2.1	Multi-Material Printers	8
2.1.1	Stratasys Objet Connex Series	8
2.1.2	Fab@Home.....	8
3	Design Goals	11
3.1	Balance Between Cost and Quality.....	11
3.2	Modular and Open Architecture.....	12
3.3	Multi-Material Printing	13
4	Design.....	15
4.1	Distribution of Motion Axes	15
4.1.1	Arrangement of the Axes	15
4.2	Design of a Linear Motion Axis	18
4.2.1	Linear Guides	18
4.2.2	Transmission.....	20
4.2.3	Actuators.....	21
5	Hardware Implementation	24
5.1	X- and Y-Axes Overview	24
5.2	X-Axis Details.....	27
5.3	Y-Axis Details.....	29
5.4	Z-Axis Overview	31
5.5	Z-Axis Details	32
5.6	Modular System.....	36
5.7	Print Heads	38
5.8	Electronics and Wiring	39
5.9	Frame and Enclosure	40
6	Controls System Implementation	43
7	Results.....	50

7.1	Bas-Relief Coin	50
7.2	Multi-Material “Dots”	52
8	Conclusions	54
8.1	Extensions / Future Work.....	54
	Bibliography	55
	Appendix A: Measuring the Maximum Acceleration of the X-Axis	57
	Appendix B: MATLAB Code.....	58
	Appendix C: Bill of Materials.....	60

1 Introduction

Additive manufacturing is rapidly finding a variety of applications in producing objects with complex geometries. In particular, as 3D printers build up the final object from raw materials rather than starting with a monolithic piece of stock, the material composition of the object being fabricated can be varied, resulting in a multi-material object. This technique can be used to produce objects with non-uniform mechanical properties and internal structures such as conducting traces. However, few available additive manufacturing technologies support the use of multiple materials in the same object; those that do are closed-source and expensive, making development of new materials and applications expensive.

This thesis presents the design of a 3D printer to address these concerns. The printer has the following qualities:

- **Multi-Material:** The printer uses inkjet print heads to dispense build materials, allowing for the production of objects composed of more than one type of material.
- **Low-cost, high-resolution:** The printer is intended to supply print quality approaching that of industrial 3D printers, with a price only a few times that of current desktop printers.
- **Modular:** The print heads are attached to the printer using a modular system, allowing the use of multiple types of print heads as well as the development of print heads independent of the printer's positioning system.

First, in Section 2 an overview of existing multi-material 3D printers is presented. Next, the motivation for the development of a new type of 3D printer is discussed in Section 3, with an emphasis on addressing the shortcomings of current 3D printers. The design of the motion system is presented in Section 4 along with alternative designs, their benefits, and their shortcomings. The implementation of the design is presented in Section 5 and the design and implementation of the controls system is described in Section 6. Next, in Section 7 sample output from the printer is analyzed, including small multi-material structures. Finally, future work aimed at increasing the capabilities of the printer is discussed in Section 8.

2 Background

Traditional computer-aided manufacturing typically involves starting with a piece of raw material, such as metal or wood, and machining away material until the final shape is achieved. As material is always being removed during these processes, conventional machining can be thought of as *subtractive manufacturing*. In contrast, *additive manufacturing* consists of joining raw material until the final shape is achieved. Although the technology dates back several decades, in recent years additive manufacturing, commonly known as “3D printing”, has become more widespread [1].

Fundamentally, all 3D printers follow the same basic process. Initially, the user creates a model of the desired object using 3D modeling software, as would be done in preparation for conventional computer-aided manufacturing. The printer’s software then takes in the digital model and converts it to a number of parallel “slices”. These slices are representations of cross-sections of the object. The 3D printer then deposits raw material in order to produce a single slice. The printer gradually builds up the object by adding new layers of slices on top of previously deposited ones.

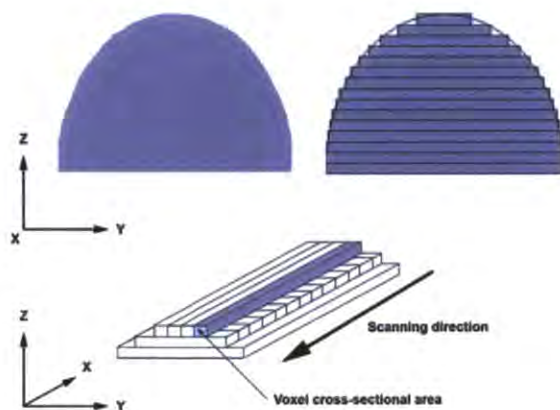


Figure 1: A depiction of the slicing process for additive manufacturing. From the Wikipedia article on 3D printing [2].

2.1 Multi-Material Printers

While multi-material 3D printing has not been extensively explored, a few examples do exist. In this section, a commercial example from Objet Geometries is presented, along with an open-source example from the Fab@Home project.

2.1.1 Stratasys Objet Connex Series

The only available multi-materials on the market today are the Objet Connex series produced by Stratasys. These printers feature excellent print resolution due to the use of inkjet print heads to dispense materials. However, their high cost makes access to this technology difficult for many research labs and hobbyists. In addition, the closed-source nature of the printers means that development of new materials or modifications of the printer by users is essentially impossible.



Figure 2: A Stratasys Objet500 Connex. Stratasys produces the Connex series, the only multi-material 3D printers currently on the market. Image from the Stratasys website [7].

2.1.2 Fab@Home

A previous project that attempted to address the limitations of 3D printing was Fab@Home. This project, begun in 2005 at Cornell University by Evan Malone and Hod Lipson, focused on developing a “simple, low-cost, user modifiable freeform fabrication system” (Malone and Lipson, 2007). The resulting printers, the Fab@Home Model 1 and Model 2, are low-cost, open-source designs made primarily from laser-cut plastic. The

open-source nature of the project allowed others to build and modify their own Fab@Home printers.



Figure 3: A Fab@Home Fabber Model 2. The printer is made primarily from laser-cut acrylic and features a closed-loop positioning system. Image from the Fab@Home Wiki [8].

The Fab@Home printers use syringes to dispense build materials, allowing the use of a variety of materials such as epoxies, silicones, food materials, and hydrogels. Variations on the printers include multiple-syringe print heads, allowing the fabrication of multi-material objects. Syringes can be swapped in and out of the printer, allowing the same machine to be used for printing a variety of objects.

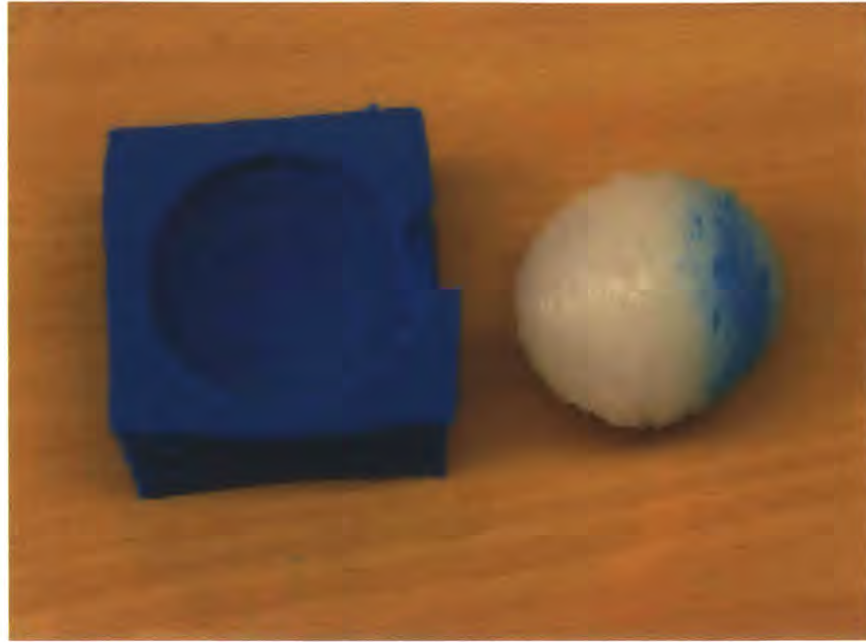


Figure 4: A silicone sphere (right) printed on a Fab@Home Fabber. Frosting was used as a support material (left). Image from Fab@Home Wiki gallery [9].

While the positioning abilities of the Fab@Home Model 2 are adequate, the use of a syringe as a dispensing tool limits the minimum feature size that can be produced. In addition, the use of acrylic as a structural material lowers the stiffness of the printer's frame, adversely affecting the print quality. Overall, the print quality of the Fab@Home printers as seen in the Fab@Home Wiki gallery is lower than other desktop printers such as the Makerbot and the Ultimaker.

3 Design Goals

Given the current shortcomings in the field of 3D printing, the current research proposes a **low-cost, modular, multi-material** 3D printer, intended primarily for research purposes. The design presented in this thesis delivers a good balance between cost and quality, as detailed in Section 3.1. The benefits of a modular design are discussed in Section 3.2. Finally, the importance of multi-material printing capabilities are presented in Section 3.3.

3.1 Balance Between Cost and Quality

The designs of 3D printers seen today reflect compromises between cost and print quality. Printers produced by traditional manufacturers such as 3DSystems and Stratasys produce high-resolution objects using mature technologies such as fused filament fabrication and stereolithography. Accordingly, these printers are expensive devices usually purchased by research labs and research divisions of companies. Their high prices (tens or possibly hundreds of thousands of dollars) typically keep them beyond the reach of typical consumers and hobbyists.

In recent years, however, a trend has begun to produce 3D printers that individuals can afford. Projects such as Makerbot [3], RepRap [4], and Ultimaker [10] have brought fused filament fabrication technology to the consumer level. In particular, the RepRap project features 3D printers built using 3D printed parts, allowing hobbyists to acquire a 3D printer at low cost from other RepRap owners. These projects have in turn inspired an endless variety of low-cost 3D printers, both in kit and prebuilt form.

However, the print quality of most of these “desktop” printers tends to be much lower than industrial 3D printers. To keep costs down, the structural components of these printers are typically made from inexpensive materials such as wood, plastic, or threaded rod; the resulting reduction in mechanical stiffness tends to adversely affect the print quality. Additionally, most kit-based printers require extensive manual assembly and calibration to function properly.

Finally, only a limited variety of 3D printing technologies is available at a low cost. Almost all hobbyist-level printers use fused filament fabrication, as it is an inexpensive and safe technology. Accordingly, this choice of technology mostly limits the available print

materials to thermoplastics such as ABS and PLA, although some hobbyists are beginning to develop other material choices [5]. In addition, due to their simplified design most low-cost printers feature only a single extrusion head. As a result, they are limited to either printing only objects that do not require support material, or to using the build material as support. Some recent projects such as the Form1 printer from Formlabs have begun to bring stereolithography to the consumer market [6]. These printers are capable of producing parts with a much finer resolution, owing to the superior minimum feature size and layer thickness available with stereolithography. However, these printers are still at the early stages of production, so their effect on the consumer market remains to be seen.

This research focuses on keeping the cost of the printer low while delivering print quality similar to that of industrial 3D printers. As this research concerns the development of a printer, the exact cost of the final printer is hard to define. Nevertheless, an emphasis is placed on use of commercial off-the-shelf components with good performance, should the design be open-sourced in the future, allowing others to easily replicate the printer.

3.2 Modular and Open Architecture

Another issue in additive manufacturing concerns the ease of designing and testing new 3D printers and print materials. Industrial 3D printers are closed systems, usually offered with a maintenance contract from the manufacturer. As a result, it is difficult or nearly impossible to modify these printers, making development of new hardware and software difficult.

In contrast, consumer-level printers such as the Makerbot are readily modifiable. In particular, the open-source nature of the RepRap project allows users to easily modify the printer's mechanical design, source code, or support software. Accordingly, a variety of modifications have been proposed and distributed over the Internet. However, the extent of modifications to these printers is inherently limited by their design. As a result, there has been little experimentation with technologies other than fused filament fabrication.

Consequently, in order to ease development of print heads and print materials, the printer features a modular design. By providing a modular interface with which to attach print heads to the printer, the system separates the complexity of a positioning system from the development of print head systems. In addition, the modular nature of the printer

allows the use of multiple types of print heads on the same printer, allowing the same device to be used for different types of development.

3.3 Multi-Material Printing

Traditionally, when a designer desired a combination of physical properties in a single object, he or she would create the object out of a combination of parts, each part having some of the desired properties. For instance, consider a typical office chair. The chair must have sufficient structural rigidity to support a person's weight, but it must also be comfortable to sit on. Making the chair's frame out of metal fulfills the first functional requirement; making the seat and back of the chair out of padding and fabric fulfills the second.

With traditional manufacturing techniques, achieving the desired combination of physical properties is a complex task. Either a combination of parts must be used, complicating the design, or exotic materials or composites must be used, complicating the manufacturing process. As additive manufacturing works by depositing material only where it is needed, it is possible to create a single object from a combination of materials, a process known as multi-material 3D printing.

Unfortunately, most current 3D printing techniques are unable to support this capability. Stereolithography requires that the object being built be immersed in a pool of build material; as a result, the build material cannot be changed without draining the build area and flushing with solvent, a time-consuming and impractically expensive procedure. Similarly, it would be difficult to use multiple build materials in powder-based techniques such as selective laser sintering.

A 3D printer using fused filament fabrication can make use of multiple materials if it has multiple extruder heads; most commercial printers do in fact feature multiple extruders to allow the use of support material. However, comparatively little attention has been given to the use of multiple materials within a single object printed on a fused filament fabrication device, or even the use of multiple colors of filament. Part of the difficulty may lie with the mechanics of the printers' feed mechanism, which requires raw materials be fed in as long filaments.

As described in Section 2.1.1, the only commercially available multi-material printers available today are the Objet series produced by Stratasys. These printers use photopolymer inkjet technology, allowing for easy mixing of materials. These printers can use two different types of material, in addition to support material, and can produce 12 grades of “digital materials” by mixing the two source materials. The primary drawback of these printers is their high cost, as well as the high cost of their materials. In addition, as the build materials used in these printers are UV-cured, the variety of available material properties is somewhat limited. Finally, a multi-material model requires one triangular mesh file per material used, which complicates the process of creating multi-material models.

To this end, the printer presented in this research features multi-material printing capabilities. Despite the potential of 3D printing to allow the manufacture of objects featuring a variety of materials, this ability has not been extensively capitalized on in 3D printer development. The research will initially focus on the use of inkjet print heads to dispense build materials, as they offer a fine print resolution and minimum feature size.

4 Design

This section presents the design of the motion system of the 3D printer. First, the merits of particular motion axes arrangements are discussed in Section 4.1. Then, in Section 4.2 a variety of designs for linear motion axes are presented, along with the benefits and drawbacks of each and the design eventually chosen.

4.1 Distribution of Motion Axes

3D printing requires positioning a print head in three dimensions relative to a build platform: two dimensions are required to produce a single slice, and one more is required to reposition the system to fabricate additional slices on top of the first. Generating three degrees of positioning movement requires a minimum of three degrees of actuation. Theoretically, this positioning may be carried out via a number of means, such as revolute positioning arms. In practice, a typical arrangement consists of three linear degrees of actuation corresponding to the linear X-, Y-, and Z-axes of a traditional Cartesian coordinate system. While more exotic arrangements may have specialized applications, three prismatic joints usually results in a simpler motion control problem.

Since the printer's motion control system must be able to position the print head relative to the build platform, the question becomes how best to distribute actuation in the X, Y, and Z directions between the print head and the build platform. Movement in the X and Y directions occur more frequently than movement in Z; as a result, typical designs in other 3D printers, as well as the design used on this printer, move the print head in the X and Y directions and actuate the build platform only in the Z direction. This prevents the heavy build platform from being shifted excessively frequently. In addition, lateral movement of the build platform could disturb delicate parts being fabricated on top of it. Moving the platform in the vertical direction avoids these complications while requiring a less complicated design than one that moves the print head in all three directions.

4.1.1 Arrangement of the Axes

In order to position the carriage in 2 dimensions, the motions of the X-axis and the Y-axis must be combined. A typical design uses the X-axis to move the carriage; the Y-axis in turn moves the entire X-axis, supplying the second degree of freedom, as seen in Figure

5(a). This standard design is commonly used on mills, routers, and a variety of 3D printers, both industrial and desktop. However, the load for the two axes is different, as the X-axis needs only to move the mass of the carriage, whereas the Y-axis must move both the mass of the carriage and the X-axis. Consequently, the control schemes for the two axes must be different to compensate for the difference in weight, which complicates the process of following two-dimensional motion paths.

One alternative design is the “crossed axes” design, shown in Figure 5(b). This design is symmetric and works by having both the X- and the Y- axes move a single linear shaft; the carriage is located where the shafts cross each other and rides on both of them. Neither axis has to support the weight of the other or the weight of the motors, so the overall moving mass is greatly reduced.

The primary drawback with the crossed axes design is the reduction in space available at the carriage. The position where the shafts cross must house bushings or linear bearings for the design to move smoothly. Consequently, print heads would have to be mounted either well below the carriage, or to the sides of it in the “quadrants” created by the crossed shafts.

Another parallel-kinematics design is the “delta robot”, shown in Figure 5(c). This design uses linkages to transfer the motion of three actuators to the carriage [11]. Consequently, the moving mass is reduced, and the system dynamics are symmetric with respect to the actuators. In addition, this design can move the carriage in three dimensions, eliminating the need for a separate Z-axis.

However, the delta design is more complex to build as it has a large number of moving parts. In addition, there may be a significant amount of play at the carriage due to the combined play in all of the mechanical linkages. Finally, control of a delta design is complicated due to the need to solve a complex inverse kinematics problem to control the position of the carriage.

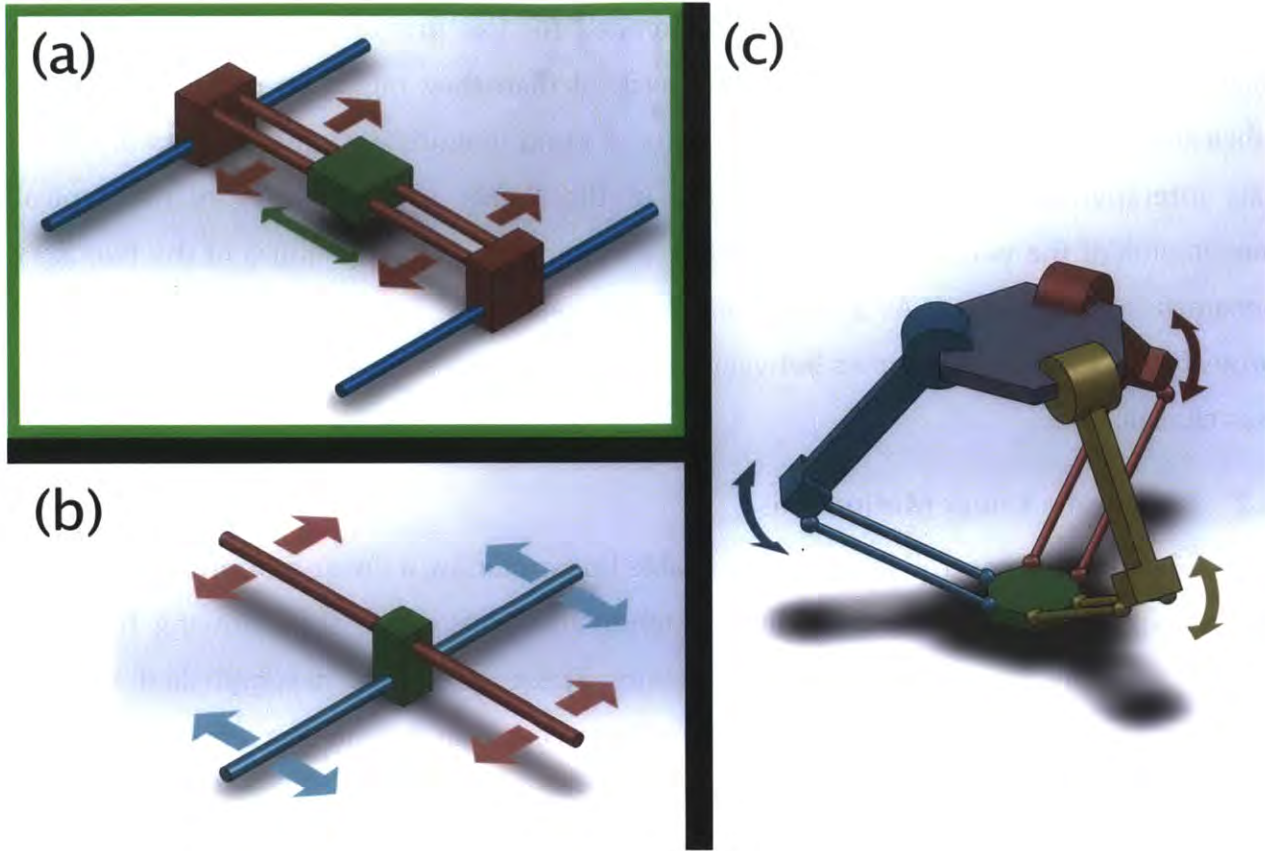


Figure 5: A series axes arrangement (a), a crossed axes arrangement (b), and a delta robot configuration (c). In each figure, the carriage being moved is shown in green. While the crossed axes and delta arrangements have superior dynamics, option (a) was eventually chosen for ease of development and increased carriage mounting space.

Consequently, there are two primary reasons that a standard serial arrangement of the axes was chosen. First, as a traditional design is compartmentalized, the X-axis and Y-axis can be developed independently, simplifying the design process. The mass of the X-axis must be known or estimated in order to select components for the Y-axis, but the design of the Y-axis is not strongly dependent on the design chosen for the X-axis. In contrast, the linked nature of the two axes in the parallel designs means that their design and implementation is more complex. Similarly, in the traditional design the axes can be assembled sequentially rather than having to align both axes simultaneously. The sequential nature of the assembly also allows for testing of the X-axis prior to assembly with the Y-axis.

Secondly, because the printer is intended for use primarily with inkjet printing technologies, balanced dynamics are less critical than they might be in fused filament fabrication. Inkjet printing primarily consists of rapid long-distance movements in the X-axis interspersed with short movements in the Y-axis. Consequently, as the typical movements of the two axes are quite different, similarity in the dynamics of the two axes becomes less important. As a result, ease of development was more important to this project than balanced dynamics between the two axes, so a standard arrangement of axes was chosen.

4.2 Design of a Linear Motion Axis

To produce controllable and repeatable linear motion, a linear motion axis must be stiff enough to resist deflections in unwanted directions while still allowing free and precise movement in the desired direction. These goals are accomplished by the combination of two components: a linear guide to constrain motion to a straight line, and an actuator to produce the motive force.

4.2.1 Linear Guides

The linear guide consists of a moving carriage that rides on a linear element called a rail. Since the carriage initially has three rotational and three linear degrees of freedom, the guide must constrain five degrees of freedom to produce the desired motion.

Traditional designs for machine tools such as mills and lathes use dovetail joints as linear guides, as seen in Figure 6(a). Dovetail joints are relatively simple, robust, and can support heavy loads. However, their high operating friction makes them poor choices for automation. In addition, achieving near-kinematic constraint of the carriage on the rail requires careful manufacturing of the mating surfaces, raising the complexity of manufacture and cost greatly.

Another alternative for a linear guide is a guide bushing riding on a round rail. Hardened round shafts are relatively easy to produce, so they are widely available in a range of lengths and sizes. Because a single guide bushing does not fully constrain the carriage, a pair of rails is usually used, as seen in Figure 6(b). The rails must be carefully aligned to avoid over-constraining the system.

A related design replaces the guide bushings of the twin rail design with linear ball bearings, pictured in Figure 6(c). Linear ball bearings create less friction and hence require less force to move than a design using sleeve bearings. However, they are more expensive than sleeve bearings and can support less weight before they fail.

An extension of the ball bearing and rail design is the linear motion rail, which consists of specially shaped hardened rails and matching linear ball bearings, shown in Figure 6(d). These designs tend to support more weight than a round rail and bearing while also delivering higher accuracy due to the shape of the rail and bearing. However, they also tend to be much more expensive. In addition, the specially shaped rails require a large flat surface to mount against.

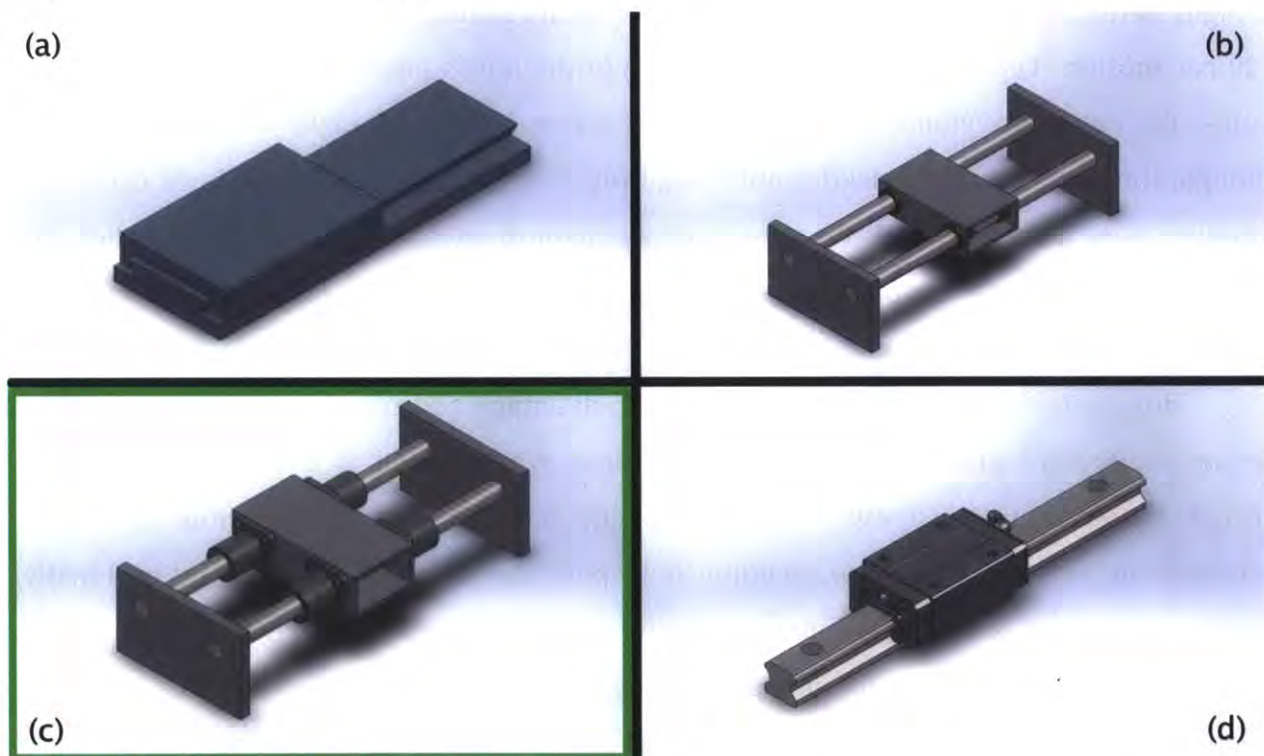


Figure 6: Dovetail rail (a), twin rails with bushings (b), twin rails with linear bearings (c), and linear motion rail (d), the four choices considered for linear guides on the printer. Option (c) was selected for its balance between cost, rigidity, and smoothness of motion.

On this printer, all three axes use twin round rails for linear guides. This design was chosen due to its good performance at relatively low cost: Properly constructed, a twin rail design provides nearly perfect kinematic constraint with easily available components. Due to the need for frequent movement in the X- and Y-axes, the carriages for those axes ride on

linear ball bearings, allowing for smooth and precise motion. Although the twin round rails are less stiff than specialty linear motion rail, the current design provides sufficient strength and precision at a fraction of the cost.

4.2.2 Transmission

Having selected the design for the linear guide, the next question became how to supply the force for actuation. As most commonly available actuators produce rotary motion, a transmission must be used in order to convert the actuator output to a desired linear motion.

One of the most commonly used linear transmissions is the lead screw drive, as seen in Figure 7(a). This design converts the relative rotary motion between a screw and nut to a linear motion. Typically, the screw turns while the nut is prevented from rotating; this causes the nut to travel along the length of the screw. If the lead angle of the screw is low enough, the design is non-backdrivable: axial forces applied to the nut will not cause the screw to turn. Leadscrews also have a large mechanical advantage, meaning that they can be used to precisely position heavy loads. As such, they are commonly seen on machine tools such as mills and lathes.

However, due to their large mechanical advantage and rotation inertia, leadscrews cannot move very quickly, limiting the maximum travel speed of a leadscrew-actuated design. In addition, leadscrews are not very efficient and generate heat due to friction between the nut and the screw, making them poor choices for frequent motion. Finally, because clearance is required between the nut and the screw leadscrews have backlash that must be compensated for using a preload force. To reduce friction and eliminate backlash, most modern machine tools use ball screws, which replace the plain nut with a ball bearing assembly that acts as a precision nut. Unfortunately, due to their greater complexity and manufacturing costs ball screws are much more expensive than ordinary leadscrews.

Another method of converting the rotary output of actuators to linear motion is a belt drive, as seen in Figure 7(b). While belt drives are usually used to transmit rotary motion between a pair of pulleys, they can also be used to produce linear motion by attaching the carriage of a linear guide to the belt. Due to their low mass, belt drives allow

for rapid precise positioning of a linear stage. In addition, by using timing belts with carefully designed tooth profiles, backlash can be almost completely eliminated.

The weaknesses of a belt drive are exactly opposite those of a leadscrew. As the mechanical advantage of a belt drive is low, they can be easily backdriven unless a holding force is applied to the drive pulley. In addition, as the belt can stretch slightly, belt drives are much less stiff than screw drives and can introduce some springiness into the system. In addition, belt drives require a tensioning system to prevent over- or under-tightening of the belt from degrading performance.

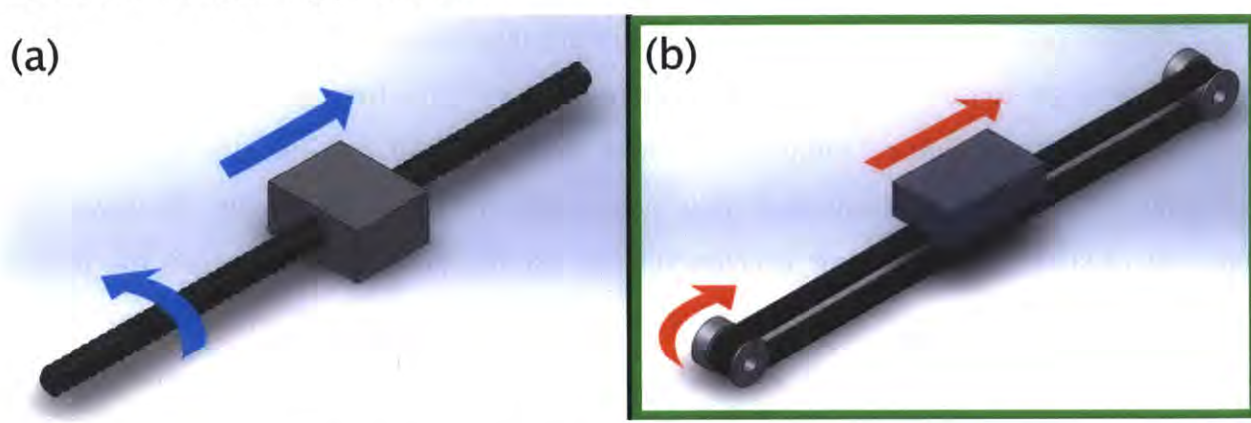


Figure 7: A screw drive (a) and a belt drive (b) were considered as transmission mechanisms. Option (b) was selected because the responsiveness of the belt drive was considered more important than the stiffness of the screw drive.

However, as this printer was designed for use with inkjet printing, the X and Y stages would have to execute rapid movements during the course of printing. Moreover, the forces during printing would be low, nullifying the primary disadvantage of a belt drive. In addition, tensioners for the belt drive proved easier to design and implement than the anti-backlash mechanism that would have been required to generate the same performance from a leadscrew. Therefore, belt drives are used on the X- and Y-axes of the printer for their responsive performance and ease of design.

4.2.3 Actuators

The final component of a linear motion axis is the actuator. On many low-cost 3D printers and CNC tools, the axes are actuated using stepper motors. The movement of a stepper motor's output shaft is subdivided into a number of fixed "steps"; when the stepper motor controller receives an input signal, the motor's output shaft will rotate through a

fixed angle and then stop and hold that position. This feature makes it possible to use a stepper motor in open-loop mode for controlling position without the need for sensors. However, the number of steps per revolution is small, typically 200, so more precise positioning applications may require a reducing transmission. An alternative method of improving positioning resolution is to use a microstepping driver, which subdivides each step of the motor into multiple smaller steps. One potential drawback with using stepper motors in open-loop mode is positioning slip: if a sufficiently high load is applied to the output of a stepper motor, the motor's shaft may stop rotating, causing the motor to "lose steps" and the positioning system to lose track of the actual position of the motor's output.

Most high-quality motion control systems use servomotors for positioning. These high-torque motors feature integrated rotary encoders and are usually used with a matching motor driver that can accurately position the motor at any angle. However, the high cost of servomotor systems precluded their use on this project: between the motor and controller, a servomotor positioning system can easily cost several times the price of a suitable stepper motor system. In particular, due to the relatively low torques required in this system, appropriately sized stepper motors supply sufficient positioning resolution and torque.

A compromise that addresses the above problem would be to use a standard DC motor to actuate the axis, paired with a linear encoder to register position – in effect, a scratch built servomotor. In addition, due to the low stiffness of a belt drive, the linear encoder is useful for verifying the actual position of the carriage, a task that cannot be performed using a rotary encoder attached to the motor's output shaft. However, non-stepper motors usually require a gearbox or other transmission to generate sufficient torque, thereby introducing backlash into the system and negatively affecting positioning performance. Low-backlash gearboxes are available, but typically add significant cost to the system. Additionally, a DC motor would require a control algorithm in order to perform the necessary position and velocity control tasks for printing.

For this project, stepper motors were found to give the best positioning ability for their cost. As servomotors were deemed too costly, the remaining decision was between stepper motors and standard DC motors. The primary weakness of a stepper motor is the potential for losing steps, but this weakness can be overcome by the addition of a linear

encoder, as would be used with a DC motor. The resulting combination is much easier to control than a standard DC motor with encoder, as low-speed positioning can be effected using open-loop positioning. In addition, open-loop velocity control can be achieved by simply feeding step commands to the motor at a constant rate. Consequently, stepper motors were chosen as actuators on this printer due to their low cost and ease of control.

5 Hardware Implementation

The following section covers specific design details of the printer's subsystems. Section 5.1 provides an overview of the X- and Y-axes, followed by detailed descriptions in Sections 5.2 and 5.3, respectively. The Z-axis design is presented in Sections 5.4 and 5.5. Next, the printer's modular system is described in Section 5.6, and the print heads presented in Section 5.7. Section 5.8 presents the electrical systems of the printer, and Section 5.9 details the printer's structural frame and enclosure.

5.1 X- and Y-Axes Overview

The X-axis and Y-axis are arranged in a series configuration to move the printer's carriage in a plane. In particular, the Y-axis carries the X-axis, which actuates the carriage, as shown in Figure 8. Both axes use a timing belt drive for actuation and ride on linear ball bearings carried on twin round shafts.

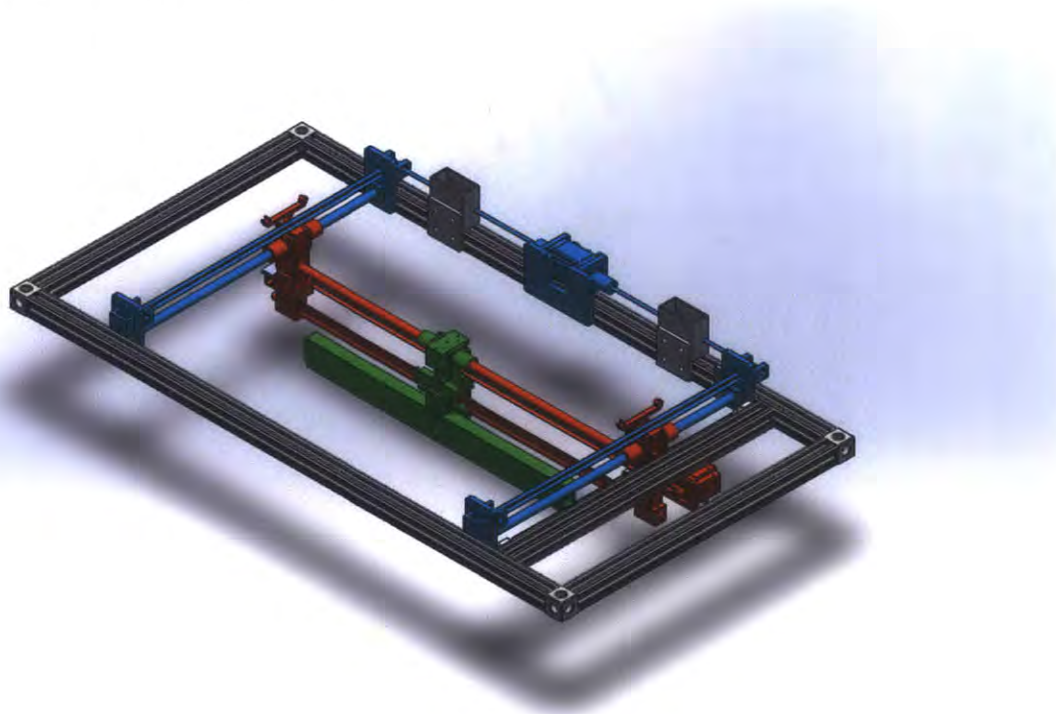


Figure 8: The Y-axis of the printer (blue) carries the X-axis of the printer (red), which in turn moves the carriage (green).

Given the functional requirements, the printer features stepper motors as the actuators on all of its axes. Stepper motors are far and away the lowest-cost option, and are capable of delivering the desired functionality. High-torque stepper motors drive the X- and Y-axis belt drives directly, allowing the printer to execute the high-speed movements required for inkjet printing. Each motor is paired with a Big Easy Stepper Driver from SparkFun Electronics, which operates in 16x microstepping mode to provide a positioning resolution better than 2000 DPI. Both the X-axis and the Y-axis feature 2mm pitch GT2 timing belt, which provide smooth engagement and low backlash.

In order to compensate for the possibility of missed steps, both the X- and Y-axes feature linear incremental encoders from US Digital. The 500 lines-per-inch encoders are used in quadrature mode, giving an effective sensing resolution of 2000 counts per inch. These encoders measure the actual position of the load being moved, thereby allowing detection of missed steps. As the encoders are a more reliable measure of the position of the printer's carriage, they are also used to trigger the print heads during printing. Finally, data from the encoders was used to compute acceleration trajectories for the X- and Y-axes, allowing for smoother movement and more accurate positioning. This algorithm is described in more detail in Section 6.

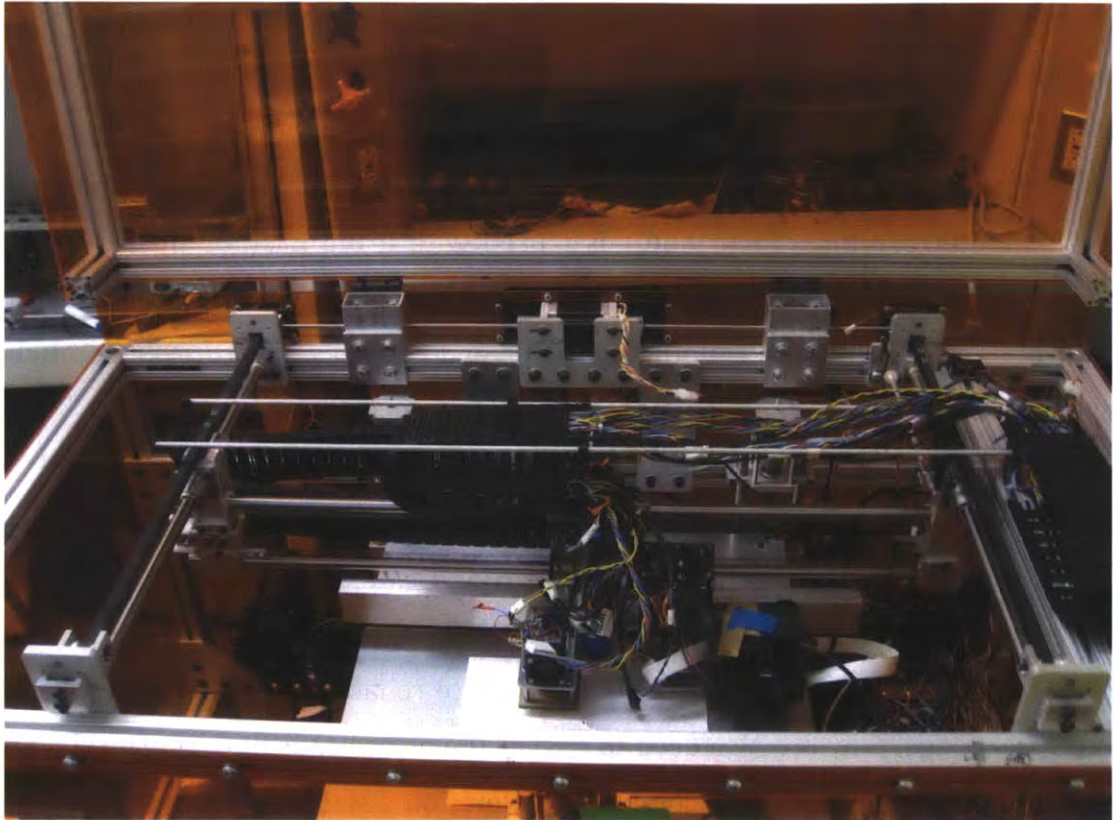


Figure 9: A view inside the printer, showing the X- and Y-axes.

5.2 X-Axis Details

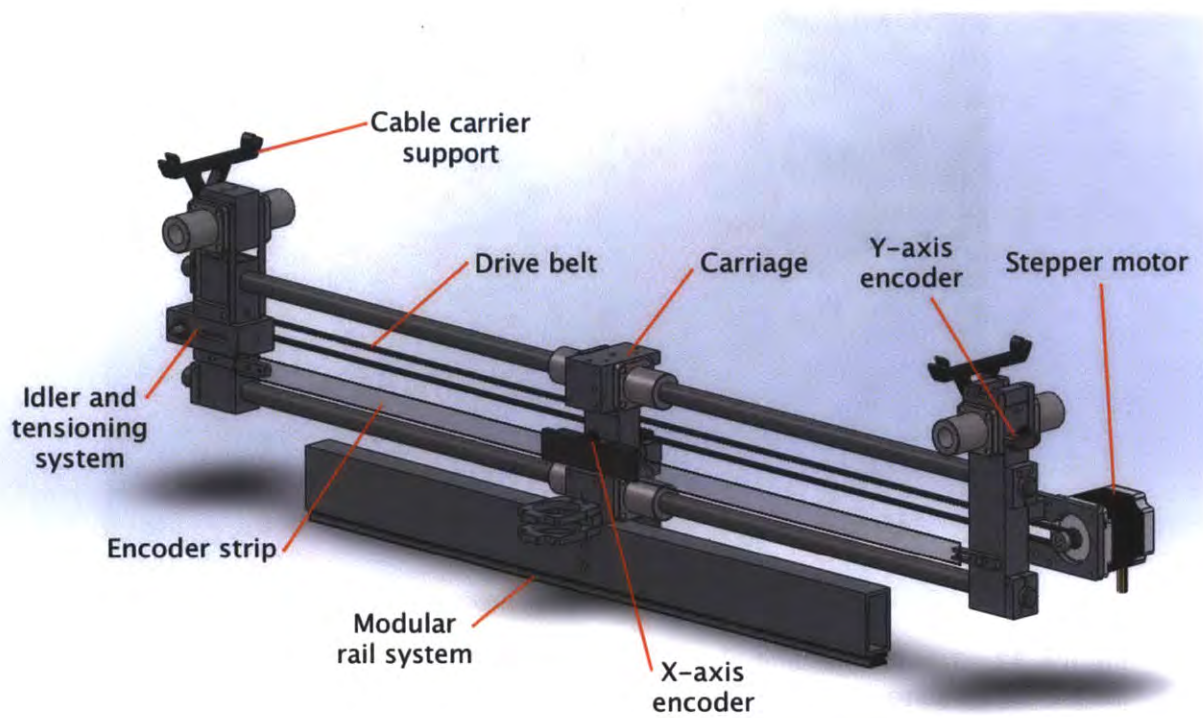


Figure 10: The X-axis of the printer. The guide rail of the modular system is visible beneath the carriage (center).

The linear guide for the X-axis is a pair of 5/8" precision-ground hardened steel shafts supported at each end by holes in aluminum box-beam extrusion. Two shafts are required to constrain the carriage to a straight-line motion. To ensure that the shafts are parallel, the support holes for the shafts were drilled and reamed through both pieces of extrusion in a single machining operation. Aluminum clamps attached to the box-beam extrusion prevent axial movement of the rods.

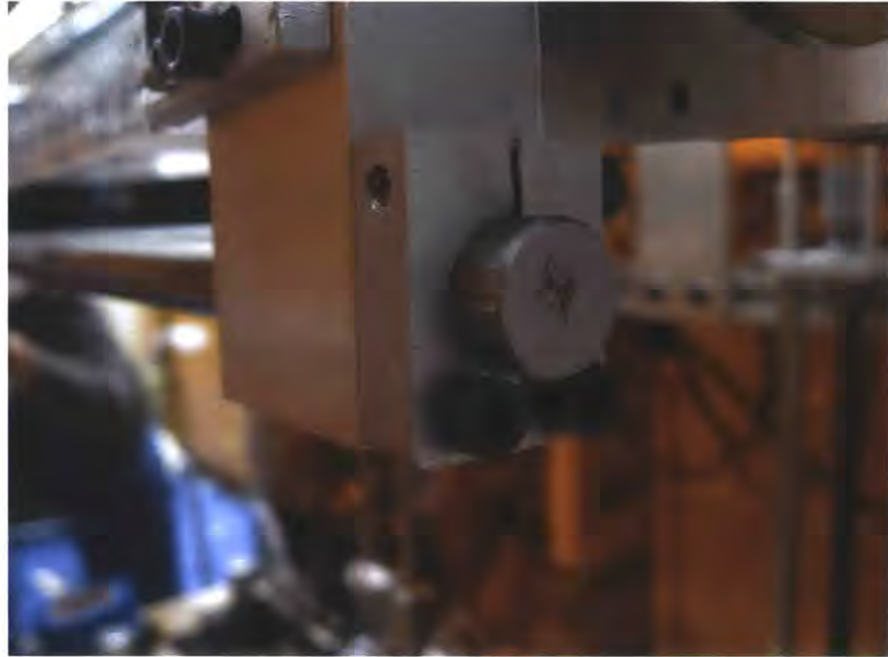


Figure 11: One of four end clamps of the X-axis guide rods. The clamps firmly secure the guide rods and prevent them from shifting axially.

The carriage that carries the print heads is machined from a block of aluminum and travels along these shafts on four flanged linear bearings. The design avoids overconstraint because the bearings can move laterally during assembly, allowing their separation to be matched to the separation between the guide shafts.

A 23Y-102D hybrid stepper motor from Anaheim Automation actuates the carriage of the X-axis via a 2mm pitch GT2 belt drive. The motor is rigidly bolted to the box-beam extrusion at one end of the axis. The other end features an idler pulley, whose position can be adjusted to change the tension in the belt. The drive belt loops around the motor and idler and is attached to the carriage with a belt clamp, thereby converting the rotary motion of the motor to linear travel of the belt.

5.3 Y-Axis Details

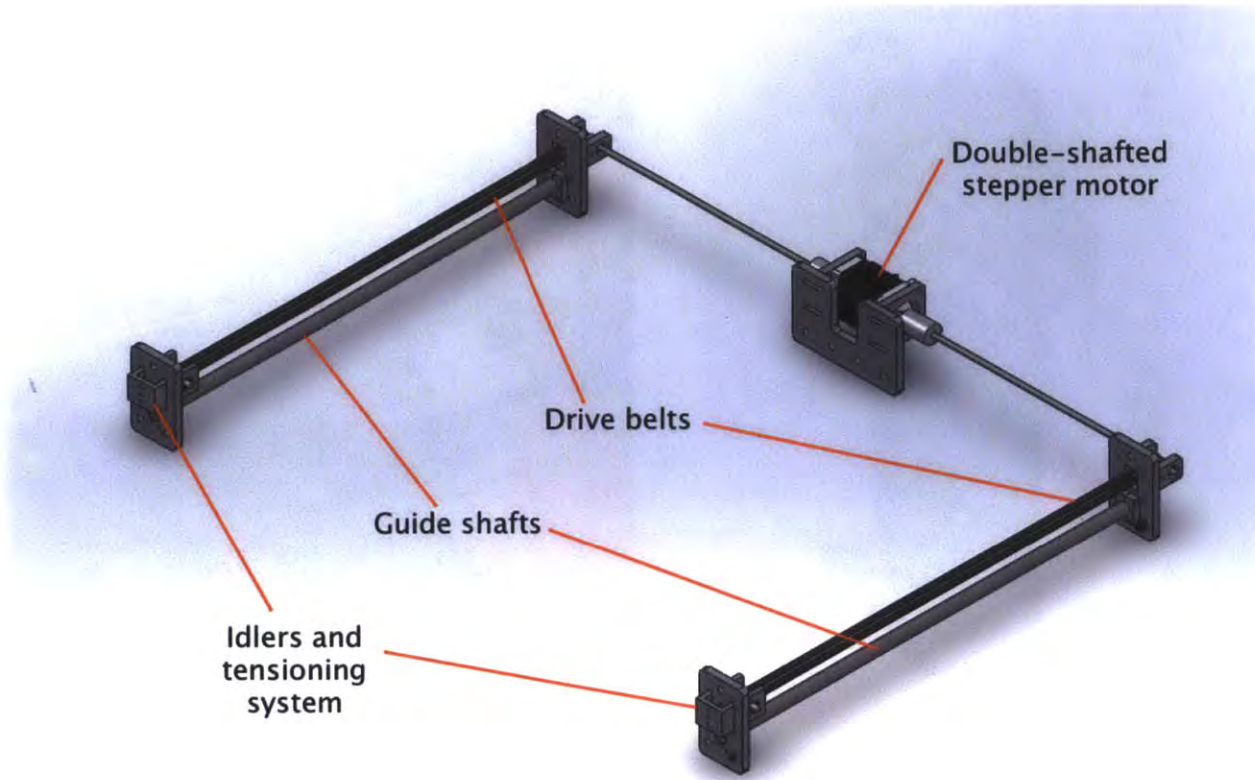


Figure 12: The Y-axis of the printer, with key components labeled. The stepper motor and the retaining plates at each end of the guide shafts are attached to the printer's frame.

As on the X-axis, the load of the Y-axis is carried on four linear ball bearings riding on a pair of 5/8" precision-ground hardened steel shafts. In this case, the load is the entire X-axis and carriage assembly, providing a second degree of translation for the printer. One pair of bearings is rigidly attached to the box-beam extrusion at the motor-carrying end of the X-axis. The other pair of bearings is attached to the idler end of the X-axis with a pair of flexures. The flexures allow the position of the bearings to shift slightly to account for misalignment of the guide shafts or thermal expansion of the X-axis.

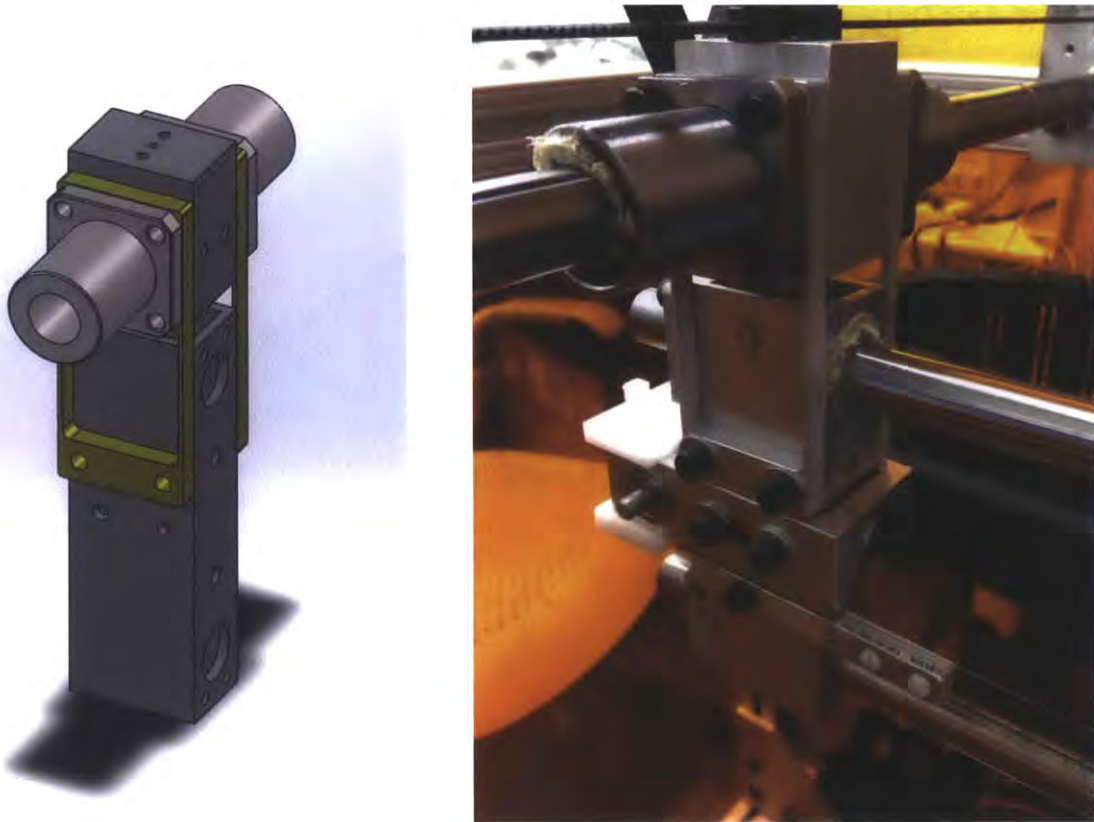


Figure 13: A CAD model of one end of the X-axis (left), showing the flexures (highlighted in yellow), and a photo of the flexures on the actual printer (right). The flexures were cut from aluminum sheet on the waterjet and allow the Y-axis bearings to shift laterally to compensate for misalignment and thermal expansion, while still supporting the weight of the X-axis.

A pair of end plates supports each shaft of the Y-axis. The two end plates for each shaft were drilled and reamed together to ensure the support holes were parallel. Aluminum clamps bolted to the end plates constrain the shafts axially. As each shaft has its own pair of end plates, the separation between the shafts is not fixed until they are bolted to the frame. This feature allows for sequential assembly of the two motion axes, as the shaft separation can be set to the length of the X-axis.

Owing to the large width of the X-axis, the Y-axis features two drive belts, one for each guide rod. Each belt has its own tensioner and is clamped on to one end of the X-axis.

A “double shafted” 24Y-404D stepper motor from Anaheim Automation is used to actuate both belts synchronously, ensuring that the X-axis is carried smoothly. The motor’s shaft extends out both sides of the case; each end connects to its corresponding belt drive

pulley via a helical beam coupling, which allows for misalignment between the motor and the drive shafts. The motor and end plates of the Y-axis are attached to the structural frame of the printer.

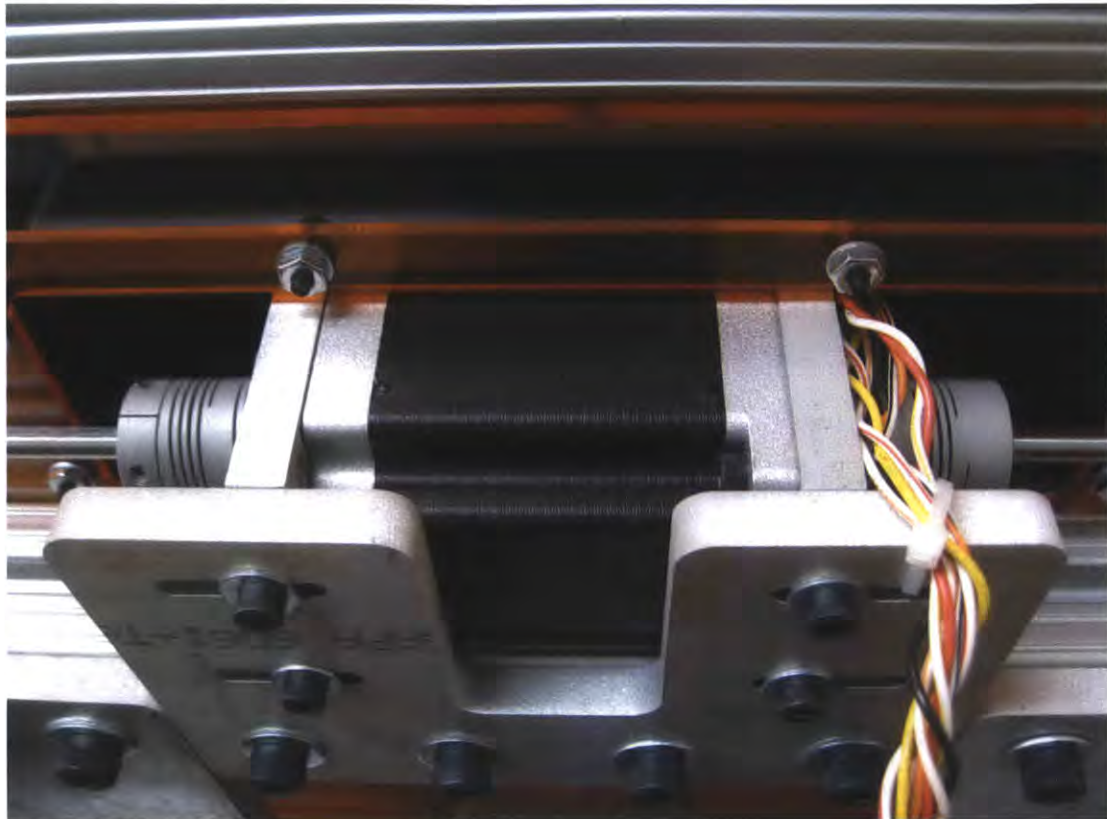


Figure 14: The double-shafted stepper motor used to actuate the Y-axis. Helical beam couplings are used to attach each end of the motor to its corresponding pulley drive shaft.

5.4 Z-Axis Overview

In contrast to the X- and Y-axes, the Z-axis only needs to make infrequent small movements: namely, each time a layer is finished, it must descend one layer in height, typically a few thousandths of an inch or less. Accordingly, low movement speed is not a concern. However, as it must support the weight of the build platform in the direction of movement, stiffness and strength are of critical importance.

A lead screw drive provides exactly the required combination of features needed for this task. The large mechanical advantage of the screw drive means even a modestly sized motor will be able to move the weight of the build platform. Screw drives are non-backdrivable, so the drive motor will not need to exert a large holding torque to maintain

the platform's position. The primary drawback of a leadscrew, the slow movement speed, is mostly irrelevant in this application because the build platform is not required to translate quickly or frequently. Finally, the backlash in the lead screw system is eliminated because the weight of the build platform preloads the drive nut against the lead screw.

Many desktop 3D printers feature a cantilevered build platform that is actuated by a single screw drive. While this design is adequate for small prints, its low stiffness makes it unsuitable for larger printers. An examination of existing industrial printers reveals that most feature two or more linear screw drives actuating the platform together, allowing multiple-point support of the build platform. Due to the size and weight of the build platform in this printer, three independent screw drives are used to control the Z-axis. The use of additional screw drives provides more support for the platform, as well as the ability to tilt the platform for leveling and calibration.

5.5 Z-Axis Details

Much like on the X- and Y-axes, the linear guide on each Z-axis screw drives is made from a pair of 5/8-inch precision-ground hardened steel shafts. The end plates of each screw drive were drilled and reamed in a single machining operation to ensure that the guide shafts would be parallel. Clamps on the end plates hold the shafts in position.

As the screw drives move more slowly and less frequently than the X- and Y-axes, their carriages ride on bronze guide bushings instead of linear ball bearings. These bushings provide a low-cost and robust alternative to linear ball bearings. The guide bushings are mounted in oversize holes and were glued into place on the carriage during final assembly of each screw drive, ensuring alignment with the guide shafts.

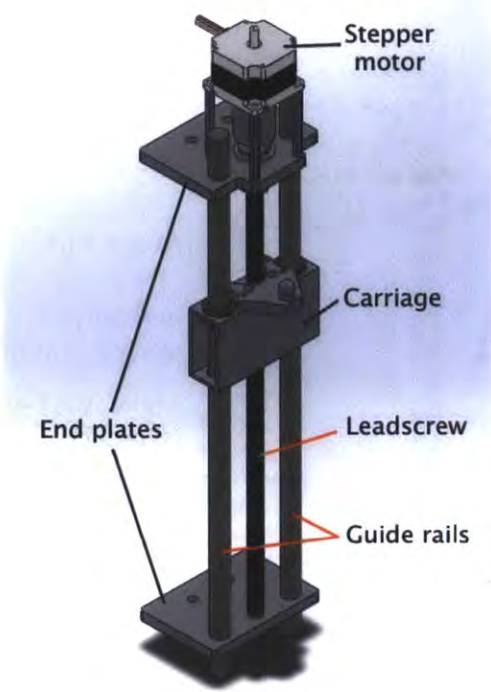


Figure 15: A CAD model (left) and photo (right) of a single screw-drive unit from the Z-axis. The motor at the top drives a leadscrew, which translates the carriage up and down. The screw drive mechanism is preloaded by the weight of the platform.

Each linear screw drive features a 23Y-002D stepper motor from Anaheim Automation at its upper end. The motor drives a $\frac{1}{2}$ "-10 acme leadscrew using a helical beam coupling, which compensates for misalignment between the motor shaft and leadscrew. A Teflon® PTFE leadscrew nut is attached to the carriage, causing the carriage to traverse linearly when the stepper motor rotates; the screw is preloaded by the weight of the build platform, removing backlash from the system. A pair of needle roller bearings at the upper end plate supports the weight on the leadscrew. Belleville washers apply a preload force to the bearings, and the entire bearing and end plate assembly is secured between two Acme nuts held in place by Loctite, as seen in Figure 16. As the lead screw "hangs" by its top end, loading forces on the screw place it in tension rather than compression, avoiding the potential for buckling.

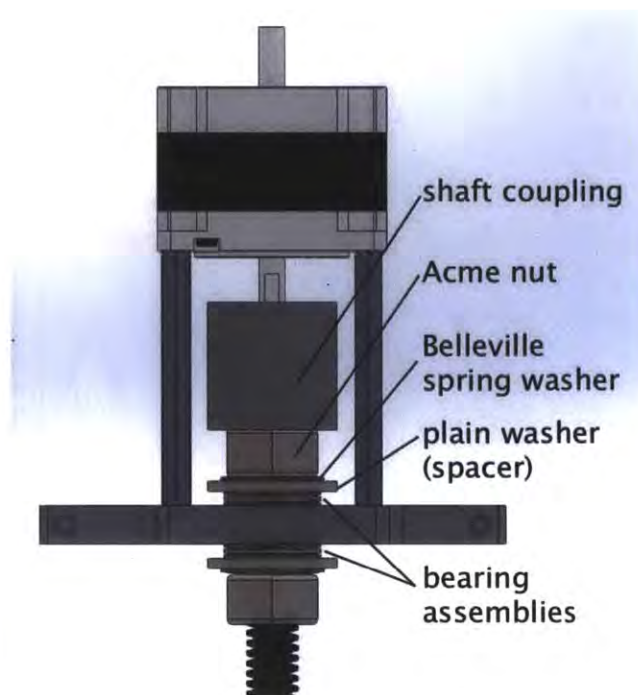


Figure 16: A close-up photo (left) and labeled diagram (right) of the top end of one of the Z-axis screw drives. The helical coupling compensates for misalignment between the lead screw and the stepper motor, while the needle thrust bearings support the weight of the platform.

The reduction of the screw drive gives each Z-axis drive unit an effective resolution of 2000 motor steps per inch of travel, even without microstepping. As a screw drive increases the effective torque of the stepper motor and is non-backdrivable, it is unlikely that the stepper motor would skip steps. Consequently, unlike the X-axis and Y-axis, the Z-axis screw drives do not feature linear encoders. However, each motor features a rear shaft for mounting rotary encoders if necessary.

Together, the three screw-drive units support the weight of the build platform. The carriage of each unit features a precision steel ball, which rides on a pair of steel shafts on the underside of the build platform. The combination of the three balls and three sets of shafts forms a kinematic coupling, precisely and repeatably locating the build platform relative to the screw-drive units. The platform is held in place by gravity. As a result, the platform can be easily removed from the printer and returned to precisely the same location. This feature potentially allows for mid-print inspections of printed parts, as well as servicing and cleaning of the build platform without re-calibration of the Z-axis. In

addition, because the three screw-drive units are independent, they can also be used to control the angle of tilt of the Z-axis. These extra degrees of freedom allow for automatic platform leveling and calibration.

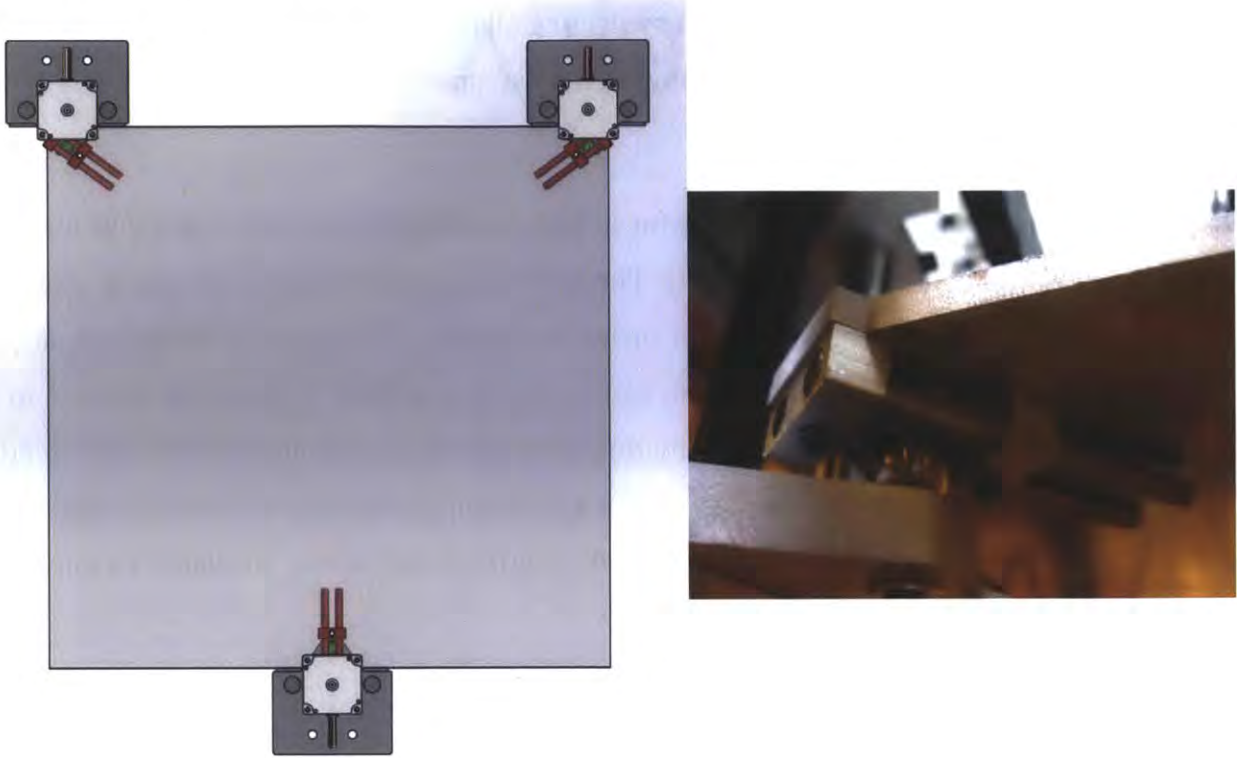


Figure 17: A top-down diagram of the build platform (left), along with a photo of the ball-and-shafts coupling mechanism (right). The diagram shows the paired shafts (red) and precision balls (green) that form the kinematic coupling that joins the platform and the screw drive units. The platform has been made transparent in this image for ease of understanding.

The build platform itself is made from a single piece of $\frac{1}{4}$ -inch thick piece of aluminum. Aluminum was chosen due to its thermal stability and good strength-to-weight ratio. In addition, it does not react chemically with most organic chemicals, making it relatively easy to clean the build platform after printing.

One potential objection to the current design is the necessity of using three independent motors to drive the three screws of the Z-axis. As only one degree of freedom is required to control the vertical axis, using a single motor to drive all three screws would be sufficient. Furthermore, synchronizing the screws using a belt or gear mechanism would keep the Z-axis from becoming misaligned after initial calibration. However, belts or gears

would exert a radial force on the screws being driven. The radial loading would necessitate a more complex design incorporating bearings to absorb the lateral forces in addition to the axial forces exerted by the weight of the platform. Finally, the synchronization afforded by a belt or gear drive can be emulated by driving all three screw drives in sync, a relatively easy task as the leadscrew drives are powered by stepper motors.

5.6 Modular System

The printer features multiple print heads, allowing the use of a variety of materials and print technologies to create objects. The printer's modular system serves to attach the print heads to the printer carriage. In order to simplify development of individual print head systems, each print head module can be easily removed from or reattached to the printer, allowing for easy testing of individual print heads or combinations of print heads.

The modular system consists of a single piece of RLA-series dovetail optical rail from Thorlabs attached to the carriage, and an optical rail carrier attached to each print head module, as seen in Figure 18.



Figure 18: The optical rail (top) and carrier (bottom). The rail is attached to the underside of the carriage, and the carriers are attached to the modules. This allows the modules to be attached and removed easily by adjusting the thumbscrew.

The optical rail is bolted to an aluminum box beam, which stiffens the rail and serves as a transition between the rail and the carriage. Although the dovetail rail does not provide exact kinematic constraint, it does provide a relatively stiff attachment point for the print head modules. In addition, both the rails and the carriers are commercial off-the-

shelf components, which allows for a relatively simple design and short development time. Furthermore, print head modules can be positioned at any location along the length of the optical rail, allowing for print heads of differing widths to be mounted to the carriage without wasting space.

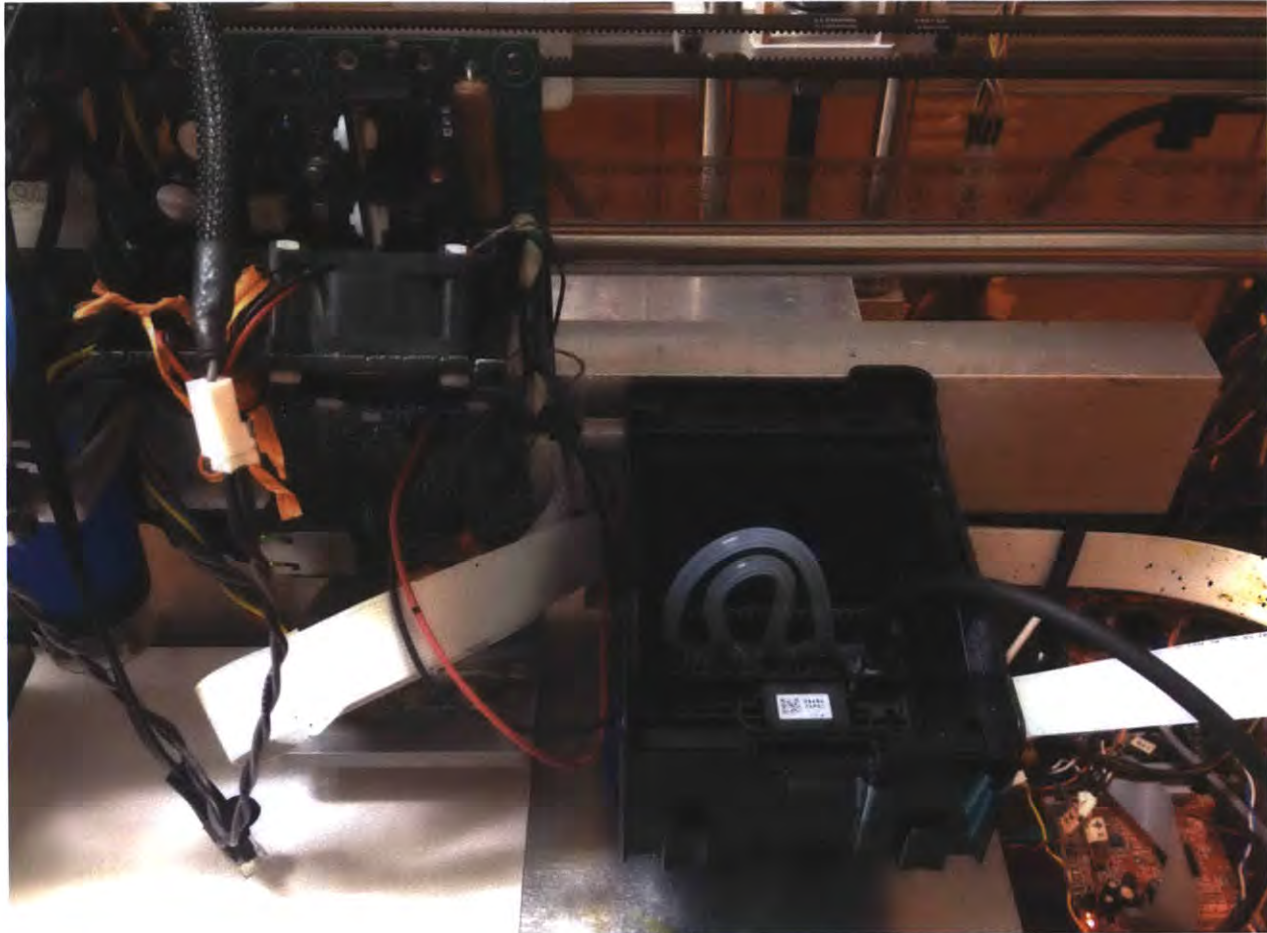


Figure 19: Two modules on the printer. The optical rail is attached to the underside of the aluminum box beam behind the module.

An alternative design features locator pins attached to each module; the pins interface with holes machined into a flat plate attached to the carriage. The modules are secured to the plate with a bolt, which provides a restraining force but does not locate the module. This design provides near-exact kinematic constraint and requires fewer expensive commercial off-the-shelf parts. However, the flat plate with mounting holes would have to be carefully machined; in addition, the spacing of the modules is rigidly

fixed, which prevents the use of modules of differing sizes. This design would be a fairly good choice for a lower-cost printer that features a smaller number of print heads.

5.7 Print Heads

Commercially available inkjet printers typically operate on one of two technologies: thermal or piezoelectric. In thermal inkjet printing, each nozzle consists of a small resistor quickly heated by a large electric current. The heat thus produced vaporizes a small quantity of ink, producing a pressure pulse that ejects a droplet of ink from the nozzle. In piezoelectric printing, each nozzle consists of a small piezoelectric actuator, which changes shape in response to high voltage. A voltage pulse fed to the piezoelectric element causes it to deform and produce a pulse of pressure in the ink, ejecting a droplet of ink from the nozzle.

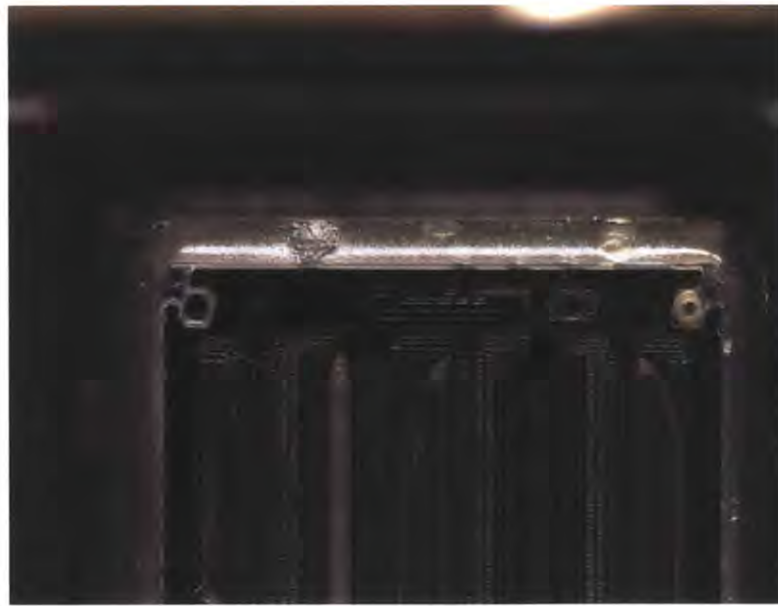


Figure 20: Close-up view of a piezoelectric print head from an Epson Workforce 30 desktop inkjet printer. Each horizontal line is an individual piezoelectric element.

While piezoelectric print heads are more difficult to manufacture and hence are more expensive than thermal print heads, they are compatible with a wider variety of materials. In particular, as piezoelectric print heads do not heat the ink, they can be used with thermally sensitive materials that would otherwise be unsuitable for use with thermal inkjets. Accordingly, piezoelectric print heads were selected for this project because they allowed for easy experimentation with a wide variety of print materials.

While industrial-scale piezoelectric print heads intended for use in poster printing do exist, they tend to be expensive and difficult to acquire. In addition, each print head features fewer nozzles and only supports a single color, complicating the process of printing with multiple materials. Consequently, the print heads used in this printer are harvested from commercially available Epson Workforce 30 inkjet printers. Inkjet printers are widely available, and provide a source of low-cost, high precision piezoelectric print heads. In addition, the ubiquity of color printing means that in almost all cases commercial print heads support the use of multiple colors of ink, meaning that multiple materials can be printed using a single print head. A custom Ethernet-enabled print head driver board was used to control the print head, as seen in Figure 19.

5.8 Electronics and Wiring

As the printer has the ability to carry multiple print heads on the carriage, a large number of cables and pipes must be routed through the motion system. These include the motor power cables for the X-axis, encoder cables, power and communication lines for the print head driver boards, and material feed lines. Cable carriers are used to organize these wires and pipes, as well as to prevent them from being tangled within the printer's mechanisms.

Two carriers are used to route electrical wires to the carriage. One carrier rests atop a structural framing element and runs parallel to the Y-axis guide rods. The Y-axis encoder wire and X-axis motor cables connect to their respective components immediately upon exiting this carrier. The second carrier is supported above the X-axis by a pair of aluminum shafts and is carried along with it when the Y-axis moves. This second carrier carries the remaining power and control cables for the print heads, as well as the X-axis encoder wire.

Finally, a third cable carrier houses tubes that supply materials to the print heads. This carrier is separate from the others both to reduce the overall size of each individual carrier and to isolate the electrical systems from the effects of a leak in the materials feed systems. In order to reach the carriage, this carrier is mounted in the carriage's plane of motion, giving it two degrees of freedom as seen in Figure 21.

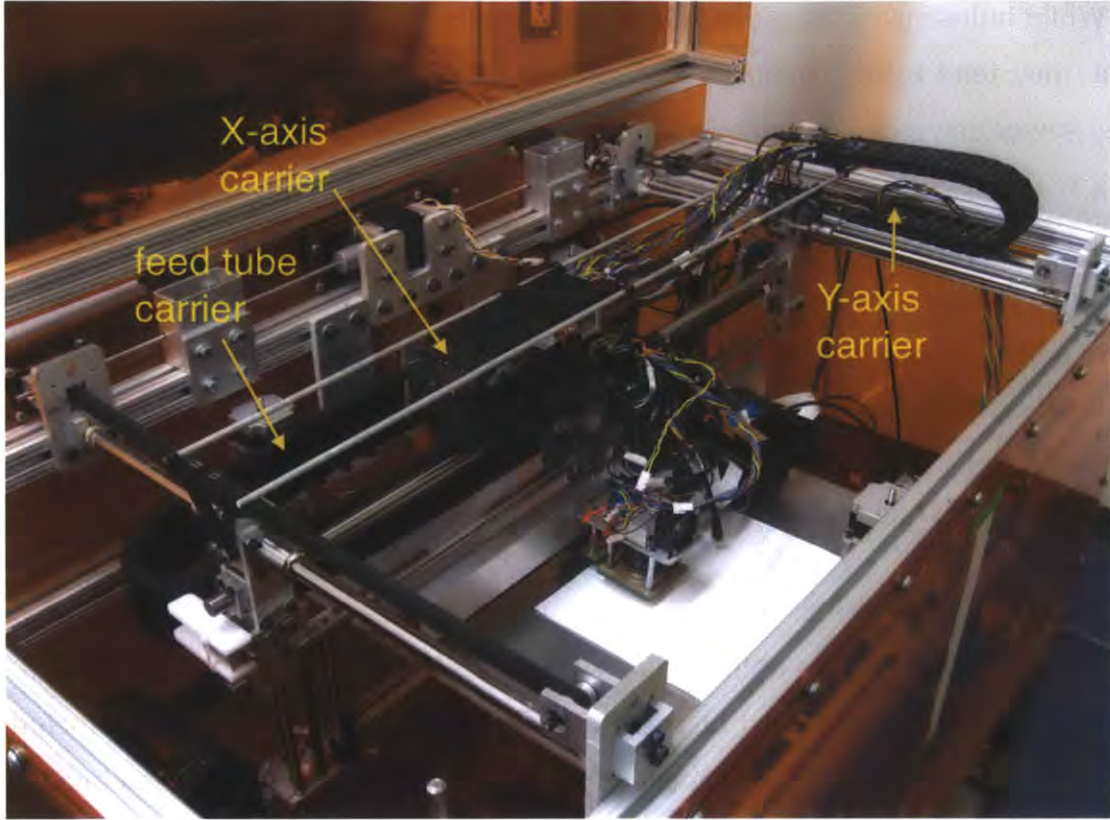


Figure 21: The three cable carriers in the printer. Cable carriers allow pipes and wires to be routed to the carriage in an orderly way without risk of entanglement or fatigue due to bending.

5.9 Frame and Enclosure

The structural frame of the printer supports the motion axes of the printer, houses the electronics, and isolates the interior of the printer from the surrounding environment. As the printer is intended for research, it is important that the frame and enclosure be simple to assemble and modify, and also allow for easy inspection of the printer's mechanical elements.

The structural frame of the printer is made from "80/20" T-slotted aluminum beams, which provides the requisite structural strength. Due to the T-slots, printer subsystems can be mounted at any point along the length of a structural framing element. Attached to the frame of the printer are UV-blocking acrylic sheets. These sheets isolate the interior of the printer from the environment, containing any volatiles or gases that are emitted during the printing process. This isolation allows the use of materials with toxic or unpleasant fumes without harming people nearby. As the panels also block ultraviolet rays,

UV-sensitive materials and photopolymers can be used as printing materials. In addition, the panels also protect individuals nearby from the UV light source used to cure photopolymers within the printer.

To improve access to the printer's internals, the upper portion of the printer's enclosure is mounted on a separate section of aluminum framing and can swing upwards to allow access to the printer's internals. Friction hinges connect the lid to the rest of the printer and hold the lid in the open position. Like the rest of the frame, the lid is covered with UV-blocking transparent acrylic panels, allowing for easy inspection of the printer's internals while the lid is closed. A safety switch disengages when the lid is opened, keeping the printer from moving or moving while the lid is open for inspection.

One potential concern when printing with potentially toxic materials, such as photopolymers, is that volatile gases may leak out through the printer, endangering people nearby. Two electric fans attached to the rear panel of the printer expel any gases or particulates produced during the printing process through a pair of exhaust ducts, as seen in Figure 22. The exhaust gases can then be vented to a chemical fume hood or captured in filters. As the exhaust fans are sufficiently powerful to lower the pressure within the print volume, outside air is pulled into the printer through any leaks, rather than exhaust gases within the printer leaking out. This system simplifies the design of the enclosure, as not every seam on the printer must be sealed perfectly.

Finally, the rear panel of the printer also features an electronics door, as seen in Figure 22. Wires pass through the printer's enclosure via this door, allowing power and control signals to be transmitted to subsystems within the printer. The door features seals that conform to wires passing through, reducing leakage of air through the door.

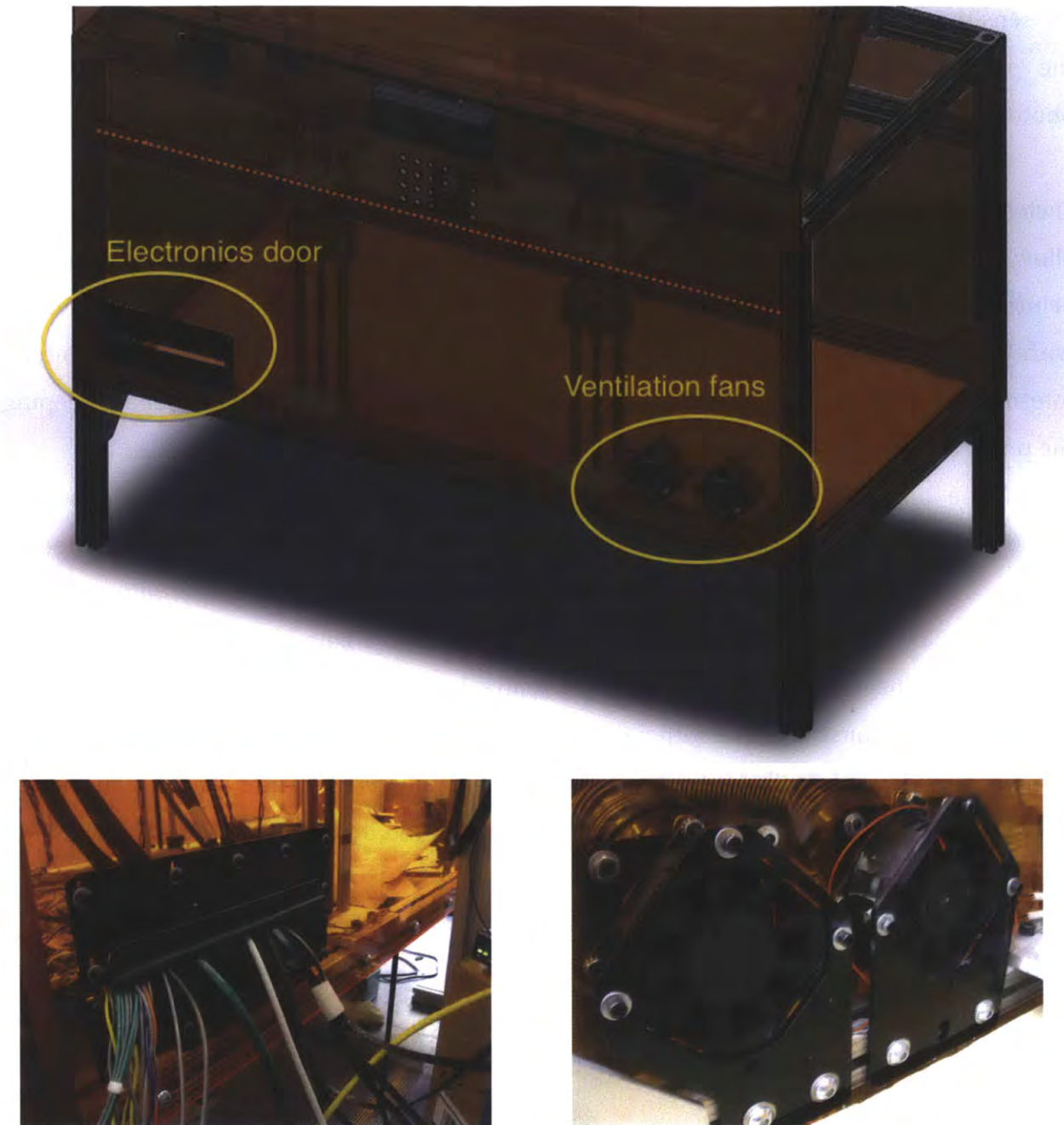


Figure 22: A rendering of the rear of the printer (top), showing the location of the electronics door (left) and exhaust fans (right). The electronics door can be adjusted to allow more wires to pass through the printer. The fans expel vapors produced within the printer to a fume hood. They also supply sufficient suction to draw air in to the printer through leaks, rather than letting gases escape the printer.

6 Controls System Implementation

As stated previously, while the printer can be used with a variety of print technologies, it has been designed with inkjet printing in mind. Inkjet printing requires the print head be placed at equally spaced intervals in rapid succession. Rather than repeatedly starting and stopping the print carriage's motion, the requirement can be more easily met by moving the carriage at a constant velocity. In particular, constant velocity movement can be obtained by feeding step commands to a stepper motor at regular intervals.

However, due to its discrete nature, a stepper motor rotating slowly may turn unsteadily. The use of a microstepping stepper motor driver allows each step of the motor to be further subdivided, allowing smoother movement. Consequently, microstepping drivers are used on all axes of this printer.

A further problem arises if a stepper motor is immediately commanded to rotate at a high speed. A stepper motor's torque decreases with increasing rotation speed, making quick accelerations to high speeds difficult without losing steps. In extreme cases, the motor's shaft may fail to rotate at all when step commands are fed too quickly to the driving circuit. In addition, sudden accelerations and decelerations of the motion system introduce impulses into the system, causing the printer to shake and the motors to lose steps.

Input shaping can be used to improve the performance of motion systems. A simple method involves linearly increasing the commanded velocity, thereby maintaining a constant acceleration. However, this approach results in step changes in the motion system's acceleration when starting, slowing, and stopping. These sudden changes in acceleration introduce impulses into the motion system, causing vibrations. A secondary effect of these impulses is to cause unsteadiness in the velocity of the carriage, betraying the assumption of constant velocity required for inkjet printing.

Consequently, a more sophisticated motion profile is used in this printer. The profile linearly increases the acceleration to its maximum value, then decreases it back to zero, while accelerating to the desired speed. The resulting velocity profile is piecewise quadratic, as seen in Figure 23.

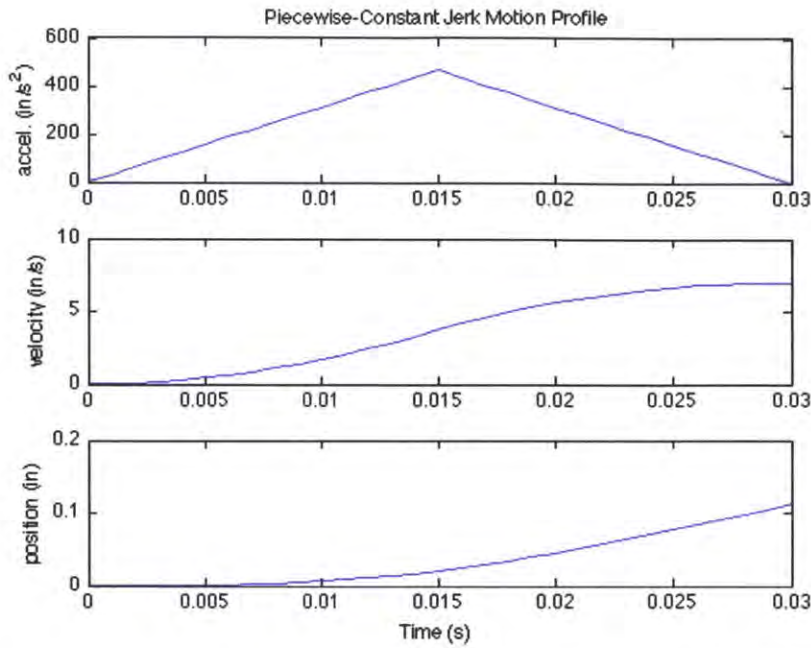


Figure 23: Acceleration, velocity, and position as a function of time using a piecewise-constant jerk profile, which linearly increases the system's acceleration to a maximum value then decreases it again.

As the stepper driver controls only the motors' positions and not their velocities, the desired velocity profile must be converted into a series of positions, known as a motion trajectory. One possibility is to use the printer's onboard processor to generate trajectories on the fly. In theory, generating motion profiles in real-time allows for the optimum profile for any given speed. However, the mathematics of profile generation may require complex processor calculations, or may even be beyond the capabilities of small embedded processors. An approximate method has been developed that are appropriate for use on embedded processors, as shown in [12]. However, implementation of that method proved difficult, even for the case of a linear velocity ramp. A linear acceleration ramp would require further complex modifications to the algorithm.

An alternative approach is to precompute the motion trajectory. As the trajectory is generated off-board, the computational load on the printer's embedded processor is significantly reduced. A more powerful computer can be used to generate the trajectory, allowing for the use of more complex input motion profiles. In addition, the task of writing computer code for trajectory generation is vastly simplified, due to the increased capabilities of off-board computers compared to the printer's embedded processor.

However, in order to support a variety of final speeds, a variety of motion profiles must be generated, potentially consuming storage space on the onboard processor. An alternative approach is to precompute only a small number of profiles, which are then rescaled or modified on the fly.

This printer uses scaled precomputed ramps for input shaping. Given a maximum allowable acceleration, a desired final velocity, and the acceleration profile shown in Figure 23, the distance required to accelerate to the desired velocity is

$$s_f = \left\lceil \frac{v_f^2}{a_{max}} \right\rceil, \quad (1)$$

where s_f is the distance in microsteps (μ steps), v_f is the desired velocity in μ steps/s, and a_{max} is the maximum acceleration in μ steps/s². As the stepper motor's velocity is controlled by the delay between steps, a velocity profile can be generated by solving for the time at which each step in the profile is reached, then taking the difference between timestamps. The total time taken by the motion profile is given by

$$T = \frac{2v_f}{a_{max}}, \quad (2)$$

where T is the time in seconds. As the acceleration increases and decreases linearly, the system follows a piecewise-constant jerk profile, with the jerk j given by

$$j = \frac{a_{max}}{T/2} = \frac{a_{max}^2}{v_f}, \quad (3)$$

where j is the jerk in μ steps/s³ and the formula for T has been substituted from (2). Using this information, during the first half of the motion profile, between $t = 0$ and $t = T/2$, the motion system follows the profile

$$s_1(t_1) = \frac{1}{6} j t_1^3, \quad (4)$$

where s_1 is the microstep count at time t_1 , $0 < t_1 < T/2$. This equation can be inverted to solve for the time t_1 of a given step during the first phase of the motion profile.

$$s_2(t_2) = -\frac{1}{6}j(t_2 - T/2)^3 + \frac{1}{2}a_{max}(t_2 - T/2)^2 + \frac{v_f}{2}(t_2 - T/2) + s_1(T/2), \quad (5)$$

where s_2 is the microstep count at time t_2 , $T/2 < t_2 < T$, j is the jerk obtained in (3), and $s_1(T/2)$ is the value for s_1 at $t_1 = T/2$, as obtained using (4). While this equation cannot be directly inverted, it can be easily solved using a numerical solver to obtain the time t_2 for a given step position, demonstrating the advantages of precomputing a motion profile. The sequence of timestamps for the steps in the first and second phases of the motion profile can be combined to give a complete third-order positioning profile for accelerating to v_f with a maximum acceleration of a_{max} . The difference between successive time stamps gives the sequence of delays between steps of the stepper motor. Reversing the sequence of delays yields the motion profile for decelerating from v_f to 0.

To obtain motion profiles for accelerating to other speeds, first a profile is generated for a chosen maximum velocity v_{max} . This profile can then be rescaled for other desired final velocities v_f by multiplying each delay by v_{des}/v_f , with $v_f < v_{max}$. As profiles for final velocities less than v_{max} accelerate more slowly, the maximum allowable acceleration a_{max} is never exceeded. Conversely, this method does not accelerate the motion system as quickly as one that always reaches the maximum acceleration a_{max} . However, the profile does require a fixed number of steps regardless of the final velocity, allowing for “acceleration zones” of known size at the limits of the motion system’s travel.

In this printer, the value for the maximum acceleration of $10^6 \mu\text{steps/s}^2$ was selected based upon experiments, as described in Appendix A. As the print heads used on the printer have a maximum firing frequency of 10 kHz, a maximum movement speed v_f greater than this yields no improvement in print speed. However, because higher movement speeds can still be useful for repositioning the carriage, v_f was chosen to be 15000 $\mu\text{steps/s}$. The generated profile was loaded onto the computer’s onboard processor,

which performs profile rescaling in real-time depending on the desired velocity. The MATLAB code used for generating the profile can be found in Appendix B.

Tests were then run to assess the effects of the ramping profile on the motion system's performance. The motion axes were accelerated to various speeds while the true position of the carriage was measured using the system's encoders. The resulting data was then compared with the system's behavior without the ramping profile. Figure 24 shows a portion of a test where the X-axis carriage was commanded to move at 10000 μ steps/s.

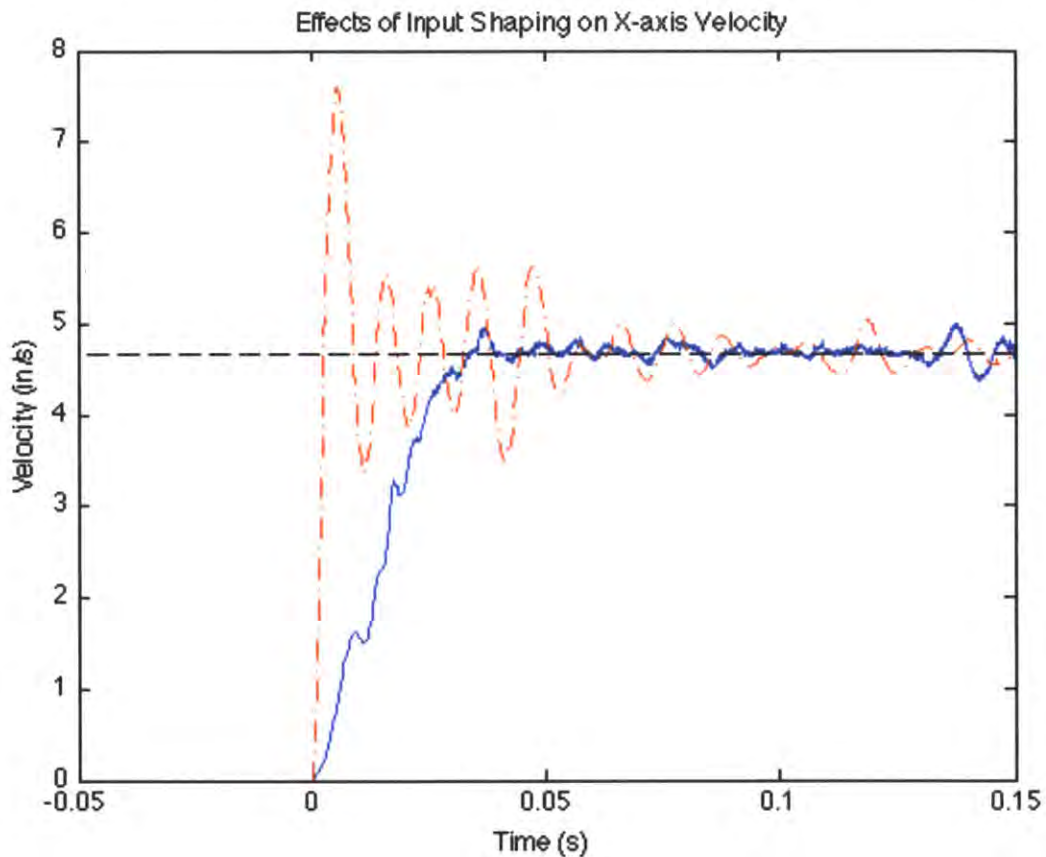


Figure 24: A comparison between the velocity of the X-axis without the ramping profile (red dashed line) and with it (blue solid line). The black dashed line shows the target speed of 4.6752 in/s (10000 μ steps/s). During these experiments, the position of the carriage was recorded using the X-axis encoder and used to calculate the carriage's velocity. The resulting velocity values have been smoothed with a moving average filter with span 10.

It can be seen that the X-axis velocity exhibits significantly less overshoot and fewer oscillations when using input shaping. The rise time is increased, but much of the increase can be accounted for by the 0.045 seconds required to execute the ramping sequence when

accelerating to 10000 μ steps/s. Additionally, during testing without input shaping the printer was observed to shake. After the addition of input shaping the printer shook significantly less. Additional evidence of the effects of the ramping sequence can be seen in Figure 25, which compares the position data from the same pair of tests. While the X-axis position rises unsteadily without the use of the ramping sequence, it increases smoothly when the ramping sequence is used.

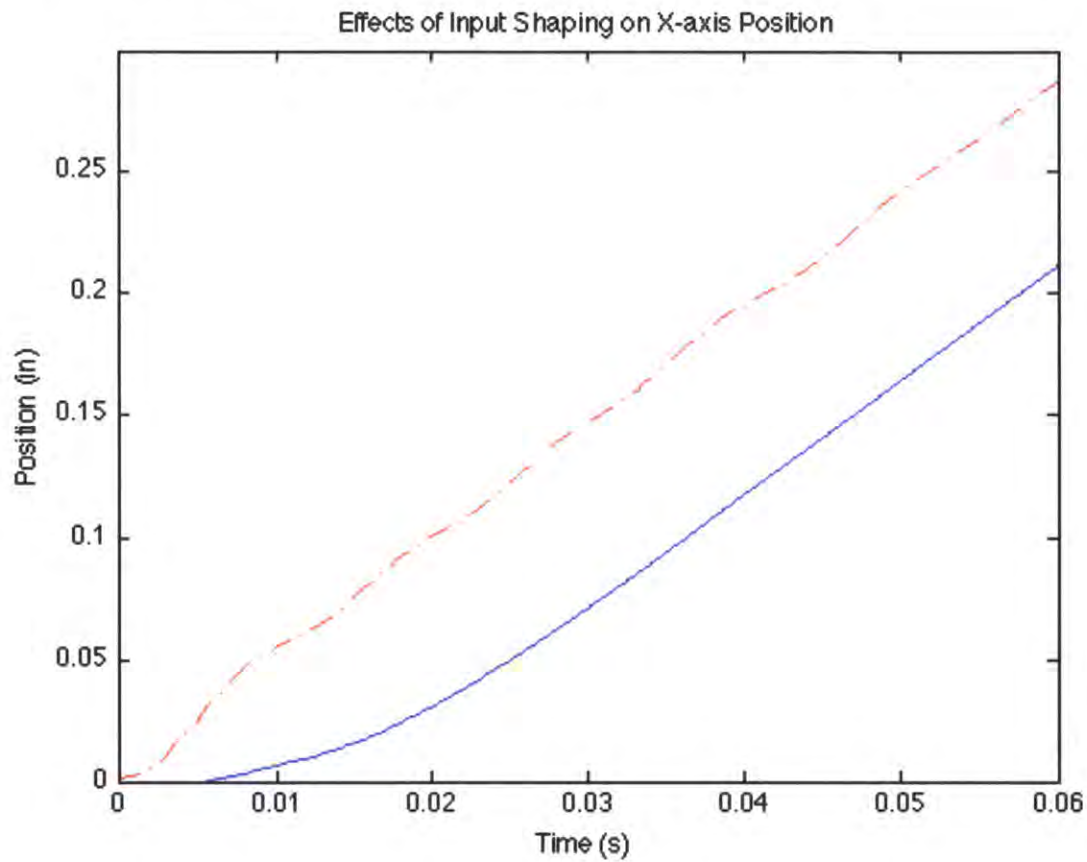


Figure 25: A comparison between the movement of the X-axis without the ramping profile (red -- line) and with it (blue solid line).

In light of the results of these tests, a similar ramping sequence has been implemented on the Y-axis, with a lower maximum v_f of 10000 μ steps/s and a_{max} of 4×10^5 μ steps/s² to account for the increased load carried by the Y-axis. This ramping sequence is only used when the Y-axis traverses large distances. For shorter movements, such as those typically performed during printing between long movements of the X-axis, there is

insufficient travel distance to execute the entire ramping sequence. Consequently, those movements are performed at a low speed to reduce induced vibrations.

Due to the low movement speed of the Z-axis screw drives, trajectory generation is not used in the control of those motors.

7 Results

Initial testing of the printer consisted of two parts: verification of the motion system, and printing test objects. Experiments with the printer's motion system were used to develop and test an appropriate input-shaping scheme for the X-axis and Y-axis, as described in the Controls System section. Current experiments focus on using the characterizing the printer's printing capabilities; testing is ongoing. Some preliminary results follow below.

7.1 Bas-Relief Coin

This object was printed using a photopolymer known as "E-20", which was developed in-house. The "coin" measures approximately 25mm in diameter, with a raised ring bearing the text "SIGGRAPH 2013" and "TWO CENTS". A profile of comedian Stephen Colbert, retrieved from [13], resides in the center of the coin. The "coin" was selected as a test object due to its relatively small thickness and variety of feature types. In addition, it can be printed without the use of support material, allowing testing without the complications of aligning the print patterns of multiple materials. The object as initially designed measured 100mm in diameter, and was reduced by a factor of 4 to expedite testing. The coin consists of 600 layers and was printed at 600 DPI.



Figure 26: A test object as designed (left) and printed using the "E-20" polymer (right). The printed object measures approximately 25mm in diameter.

Overall, small details were reproduced reasonably well. In particular, fine details of the profile such as the ear are visible, and the text on the rim of the coin is readable from a couple feet away. A few faint horizontal lines can be seen across the surface of the coin; these are artifacts produced by the nature of the printing process, as the print head is swept side-to-side to build up the object. Similar lines can be seen on prints produced by industrial printers. Key dimensions of the object as printed and as designed are compared in Table 1.

	Designed (mm)	Scaled 25% (mm)	Printed (mm)
Diameter	100	25	$24.88 \pm .04$
Ring Width	10	2.5	$2.63 \pm .13$
Thickness	8	2	$2.46 \pm .07$

Table 1: A comparison between the dimensions of the “coin” as designed and as printed; the design was scaled by a factor of 4 prior to printing. Five measurements were made of each dimension.

As printed, the diameter and ring width are fairly close to the scaled design values. However, the thickness deviates from the scaled value by almost 25%. This discrepancy can be explained by the use of an inaccurate layer thickness value during printing: As the actual layer thickness was unknown, an estimate was substituted into the software for the purposes of this test. Given that 600 layers were used during the printing, the actual layer thickness is approximately 4.1×10^{-6} m.

An additional discrepancy can be seen in the feature in the center of Colbert’s head. The brain-shaped artifact occurred as a result of print head failure during the print. Prior testing has revealed that during the course of printing, the nozzles of the print head gradually cease to eject print material, in no discernable pattern. The most likely cause is due to the viscosity of the print materials, which prevents them from flowing smoothly through the feed lines of the printer. As the print heads used on this printer were salvaged from desktop inkjet printers, they do not feature the extensive pressure and temperature sensing and control systems typically found on industrial print heads intended for use with unusual materials. Testing is currently underway to determine if the printer can be configured to operate without these systems, or if a simplified design for them is possible.

7.2 Multi-Material “Dots”

This print was intended as a test of the printer’s small-scale multi-material printing capabilities. In order to simulate the fabrication of small drug-delivery devices or pills, a series of small cuboids was printed with an outer shell made of transparent material and an inner particle of red material. The size of the inner particle gradually increases across the series of cuboids, as seen in Figure 27.

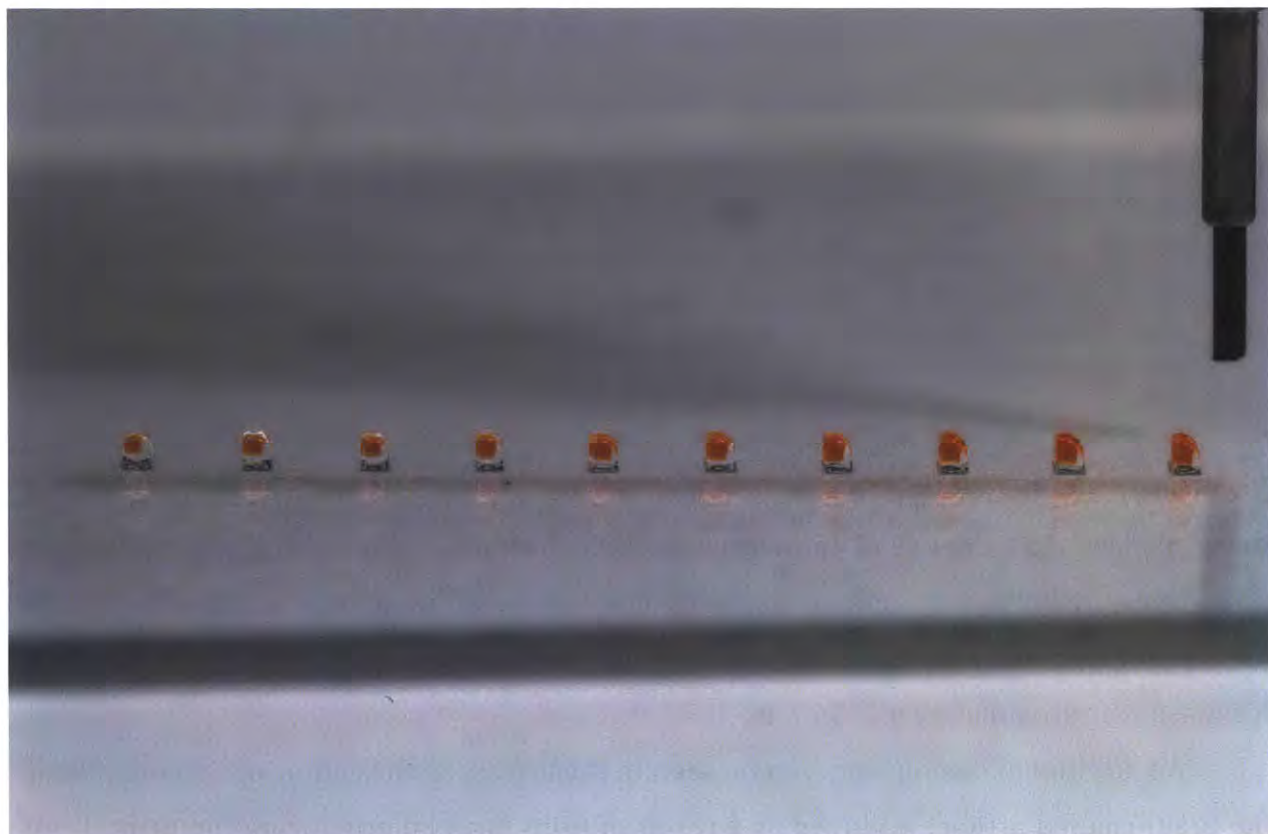


Figure 27: Multi-material “dots”. The proportion of red material in the dots increases going to the right. The mechanical pencil lead is 0.56mm in diameter.

Each cuboid was designed to be 500 μm wide and tall and consists of 114 layers. As the “dots” are small and difficult to measure physically, their size was assessed using the ImageJ image analysis program [14]. On average, the dots measure 0.49 \pm .01mm wide and 0.74 \pm .01mm tall. These values demonstrate the high-resolution and minimum feature size capabilities of the printer.

As the amount of red material decreases, the shape of the dots becomes somewhat distorted, as seen in Figure 28. There are a couple possible explanations for this

phenomenon. First, the output spectrum of the UV LED used to cure the build materials may not exactly match the sensitivity wavelength of the build materials, leading to incomplete curing and causing the dots to have a distorted shape. Subsequent versions of the UV curing module on the printer may feature alternative light sources with a broader output spectrum in order to more reliably cure all build materials. Another possibility is that the size of the jetted drops may be different between the colored and transparent materials, leading to an uneven height in the final print. Nevertheless, these “dots” provide a good demonstration of the printer’s printing resolution and multi-material capabilities.

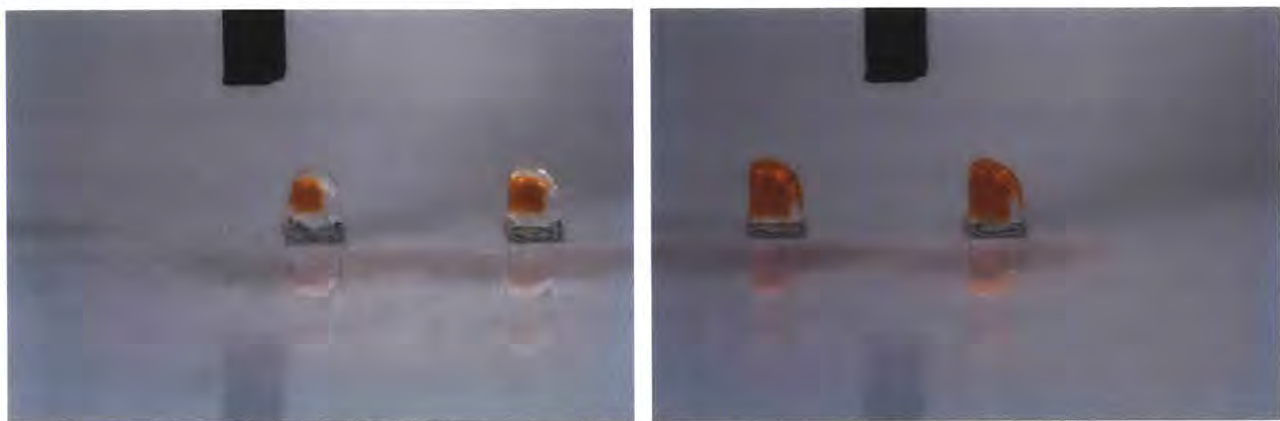


Figure 28: Photos showing the leftmost (left) and rightmost (right) multi-material dots from **Figure 27**. The distortion in shape increases with the proportion of colored material.

8 Conclusions

The printer demonstrates a robust and low-cost design using stepper motors for actuation. Commercial off-the-shelf components are used where possible, such as in the framing and linear guide systems, reducing the cost and complexity of the system without sacrificing performance. In particular, the print heads currently used on the printer are the same as those used in commercial desktop inkjet printers, allowing for high-resolution, multi-material performance in a small package at the fraction of the cost of industrial inkjet print heads. Additionally, the modular nature of the print head mounting allows for the independent development and testing of print heads.

As of the latest testing, the printer is capable of producing small high-resolution multi-material objects, as seen in the results section. In addition, the printer is capable of producing fine details, such as the lettering around the rim of the coin in Figure 26. These features allow experimentation and development of additional applications for multi-material printing.

8.1 Extensions / Future Work

Currently, the selection of print materials is limited, as development of materials is still ongoing. In particular, many photopolymers that have been tested suffer from excessive viscosity, so the print heads currently used on the printer are unable to eject them. Other polymers do not cure completely under the current UV LED module. Alternate curing modules may be developed to address this problem, either by using LEDs with different frequencies or a broad-spectrum UV lamp.

In addition, the print head currently draws material from repurposed ink cartridges. Consequently, the maximum print volume is restricted by the amount of material that can be carried on the carriage in those cartridges. By attaching the cartridges to a constant-level feed system, materials can be continuously supplied to the print head via external tanks, allowing for longer prints and larger printed objects.

Bibliography

- [1] Lipson, Hod and Melba Kurman. *Fabricated: The New World of 3D Printing*. Indianapolis: John Wiley and Sons, 2013.
- [2] Wikimedia Foundation. 2013. *3D Printing*.
http://en.wikipedia.org/wiki/3D_printing (accessed March 14, 2013).
- [3] Makerbot Industries. 2013. *MakerBot Replicator™ 2 Desktop 3D Printer*.
<https://store.makerbot.com/replicator2.html> (accessed March 10, 2013).
- [4] RepRap project. 2013. *RepRap - RepRapWiki*.
http://www.reprap.org/wiki/Main_Page (accessed March 10, 2013).
- [5] Parthy, Kai. 2013. *Print wood now - with tree rings! LAYWOO-D3 mm filament by Kaipa - Thingiverse*. <http://www.thingiverse.com/thing:30552> (accessed March 10, 2013).
- [6] Formlabs. 2013. *Formlabs - High Resolution Desktop 3D Printer*. <http://formlabs.com> (accessed March 11, 2013).
- [7] Stratasys Ltd. 2013. *Objet500 Connex Multi-Material 3D Printer*.
<http://www.stratasys.com/3d-printers/design-series/precision/objet-connex500> (accessed April 17, 2013).
- [8] Fab@Home Project. 2012. *Main Page - Fab @ Home*.
<http://fabathome.org/wiki2/wiki.html> (accessed March 11, 2013).
- [9] Fab@Home Project. 2011. *Fab@Home:Gallery*.
http://fabathome.org/wiki2/fab_home_gallery.html (accessed February 20, 2013).
- [10] Ultimaker. 2012. *Ultimaker / the fast, easy to build, affordable 3D printer - 3D printing for everyone!* <http://www.ultimaker.com> (accessed April 10, 2013).
- [11] Sogeva, S.A., Pascal Demaurux, and Marc-Oliver Demaurex. *Device for the movement and positioning of an element in space*. US Patent 4,976,582, filed September 6, 1989, and issued December 11, 1990.
- [12] Austin, David. 2005. *Generate stepper-motor speed profiles in real time*.
<http://www.embedded.com//showArticle.jhtml?articleID=56800129> (accessed April 3, 2013).
- [13] Glachant, Mathieu. 2011. *Stephen Colbert's Peabody Award! by syvwlcch - Thingiverse*.
<http://www.thingiverse.com/thing:9141> (accessed April 3, 2013).

- [14] National Institute of Health. 2004. *ImageJ*. <http://rsb.info.nih.gov/ij/> (accessed April 3, 2013).

Appendix A

Measuring the Maximum Acceleration of the X-Axis

In order to produce the motion profiles described in the Controls System section, a maximum value for the acceleration of the X-axis had to be selected. Ideally, this value is based upon the actual maximum acceleration achievable by the motion system. The holding torque of the stepper motor and the mass of the carriage can be used to calculate a value for the acceleration, but this value is inaccurate as the available torque of a stepper motor decreases with stepping frequency. In addition, nonlinear effects such as friction from ball bearings and other components may be present in the system, causing further deviation from estimated values. Thus, it was deemed easier to determine the maximum acceleration experimentally rather than simply attempting to calculate it.

The trajectory generation algorithm chosen for this project requires a chosen maximum velocity, which in the final implementation is 15000 μ steps/s. To measure the maximum achievable resolution at this velocity, the X-axis stepper motor was commanded to run at this speed without any ramping. The X-axis encoder was then used to measure the resulting motion path of the carriage. The data was then fit to a quadratic polynomial, under the assumption that the carriage could be modeled as a mass moving under uniform acceleration. This analysis yielded a value for the acceleration of 1065.8 in/s² ($R^2 = .99949$), or approximately $2.28 \times 10^6 \mu$ steps/s². For a conservative estimate, this measured value was approximately halved to yield $10^6 \mu$ steps/s², which was used in the calculations for trajectory generation.

A similar technique was used to select the maximum acceleration value used on the trajectory generation for the Y-axis.

Appendix B

MATLAB Code

The following code was used to generate the motion trajectories for the X- and Y-axes, as described in Section 6.

```
% generates a precomputed ramp to vel with max acceleration accel
% takes in v_f in steps/sec, max acceleration in steps/sec/sec
function [t, s] = precompute2ndOrdRamp(v_f, a_max)
    s_f = ceil(v_f^2 / a_max); % final position
    fprintf(1, 'total steps: %d\n', s_f);
    fprintf(1, 'about %g inches\n', s_f * 19 * (2/25.4) / 3200);

    T = 2*v_f/a_max; % total time, seconds
    jerk = a_max^2 / v_f; % calculate jerk

    s_m = ceil(v_f.^2 / (6*a_max)); % calculate halfway position
    v_m = v_f/2; % velocity at halfway time (half of final velocity)

    % concave section
    s_p1 = [0:s_m]'; % motor moves one step at a time
    % speed is controlled by time difference
    % between steps

    t_p1 = (6*s_p1 / jerk) .^(1/3); % time of each step in concave
    % section is just the appropriate
    % points on a cubic curve

    % convex section
    s_p2 = [(s_m+1): s_f]'; % remaining steps until final step position
    t_p2 = zeros(length(s_p2),1); % initialize time vector for convex
    % velocity portion

    s_m_true = v_f.^2 / (6*a_max); % calculate non-truncated halfway position

    %syms t2
    for i=1:length(s_p2)
        a = -jerk/6; % t^3 term (jerk)
        b = a_max/2; % t^2 term (acceleration)
        c = v_m; % t term (velocity)
        d = s_m_true-s_p2(i); % constant term (position)

        tvals = roots([a, b, c, d]); % solve cubic for time associated
        % with position (d)

        t_p2(i) = tvals(3)+T/2; % shift by halfway time
    end

    % comparison vectors with intended trajectory
    dt = 0.0001; % fine level time difference
    tc = [0:dt:t_p1(length(t_p1))]; % time vector for comparison
    sc = jerk/6 * tc.^3; % comparison position during first half
```

```
sc2 = sc(length(sc)) + v_m*tc + a_max/2 *tc.^2 - jerk/6*tc.^3;
% comparison position during second half

t = [t_p1; t_p2]; % output associated times
s = [s_p1; s_p2]; % output position

figure(3);
% plot generated position with intended trajectory for comparison
plot(t, s, 'b.', tc, sc, 'r', tc+T/2, sc2, 'g');

end
```

Appendix C

Bill of Materials

This appendix lists the commercial off-the-shelf parts used in the construction of the printer. In addition to these components, various thicknesses of aluminum plate and some aluminum box beam were used to form structural elements of the printer.

Frame

Part #	Part Name	Vendor	Quantity
-	1515-Lite T-slotted extrusion, 24" long	80/20 Inc.	7
-	1515-Lite T-slotted extrusion, 48" long	80/20 Inc.	8
-	1515-Lite T-slotted extrusion, 36" long	80/20 Inc.	6
-	1515-Lite T-slotted extrusion, 4.5" long	80/20 Inc.	4
47065T156	Aluminum Inch T-Slotted Framing System Concealed 90 Degree Connector, for 1-1/2" Extrusion	McMaster-Carr	4
47065T51	Aluminum Inch T-Slotted Framing System Extended 90 Degree Bracket, Sngl, 4-Hole, for 1-1/2"	McMaster-Carr	2
47065T178	Aluminum Inch T-Slotted Framing System 90 Degree Plate, Single, 5-Hole, for 1-1/2" Extrusion	McMaster-Carr	16
47065T149	Double End-Feed Fastener, for 1-1/2" Aluminum Inch T-Slotted Framing System, packs of 4	McMaster-Carr	12
6111K83	Swivel Leveling Mount Znc-Pltd STL, W/Pad, 3/8"-16 X 2" L Thrd, 2800#Load	McMaster-Carr	4

Carriage

Part #	Part Name	Vendor	Quantity
A 6M51M090	Polycarbonate Belt clamp for single and double sided belts	SDP-SI	1
6483K64	Steel Flange-Mount Linear Ball Bearing Square Flange, 5/8" Shaft Dia, 1-1/2 O'all Lg	McMaster-Carr	4
RLA2400	Imperial Dovetail Optical Rail, 24"	Thorlabs	1
RC2	Extended Rail Carrier, 1" x 2", #8-32 Tapped Holes, 1/4" Counterbore	Thorlabs	8

X-Axis

Part #	Part Name	Vendor	Quantity
ROB-10735	Big Easy Driver	SparkFun Electronics	1
23Y102D-LW8	NEMA 23 double-shaft stepper motor, 175 oz-in	Anaheim Automation	1
6061K151	Hardened Precision Steel Shaft 5/8" Diameter, 24" Length	McMaster-Carr	2
A 6A51-019DF0908	GT2 (2MM) Pitch, 19 Teeth, Aluminum Alloy Timing Pulley	SDP-SI	2
A 6R51-M680090	GT2 (2mm) Pitch, 680 Teeth, 9mm (.354)inch Wide Neoprene Belt	SDP-SI	1
A 6M51M090	Polycarbonate Belt clamp for single and double sided belts	SDP-SI	1
88935K111	Architectural Aluminum (Alloy 6063) Rect Tube, 1-1/2" X 3", 1/4" Wall Thk, 1' Length	McMaster-Carr	1
6383K214	Steel Ball Bearing Flanged Open for 1/4" Shaft Dia, 7/8" OD, 5/16" W	McMaster-Carr	2
1327K113	Miniature 12L14 Drive Steel Shaft 1/4" OD, 3" Length	McMaster-Carr	1
6483K64	Steel Flange-Mount Linear Ball Bearing Square Flange, 5/8" Shaft Dia, 1-1/2 O'all Lg	McMaster-Carr	2
6489K51	Self-Aligning Linear Ball Bearing Closed, for 5/8" Shaft Diameter	McMaster-Carr	1
9968K25	External Retaining Ring for Linear Bearing for 1-1/8" Bearing OD	McMaster-Carr	2
EM1-0-500-N	EM1 Transmissive Optical Encoder Module, 500 LPI	US Digital	1
LIN-500-36-N	LIN Transmissive Linear Strip, 500 LPI, No Index	US Digital	1

Y-Axis

Part #	Part Name	Vendor	Quantity
ROB-10735	Big Easy Driver	SparkFun Electronics	1
23Y202D-LW8	NEMA 23 double-shaft stepper motor, 262 oz-in	Anaheim Automation	1
6208K511	Aluminum Helical Beam Clamp-on Shaft Coupling 1/4" X 1/4" Bore, 1-1/2" Length, 1" OD	McMaster-Carr	2
8632T139	D-Profile Shaft 1045 Steel, 1/4" OD, 12" Length	McMaster-Carr	2
A6A51-019DF0908	GT2 (2MM) Pitch, 19 Teeth, Aluminum Alloy Timing Pulley	SDP-SI	4
A6R51-M680090	GT2 (2mm) Pitch, 680 Teeth, 9mm (.354 inch) Wide Neoprene Belt	SDP-SI	2
A 6M51M090	Polycarbonate Belt clamp for single and double sided belts	SDP-SI	2
57155K304	Mini HI-Precision SS Ball Bearing - ABEC-5 Flanged Open, 1/4" ID, 1/2" OD, 1/8" Width	McMaster-Carr	8
6061K151	Hardened Precision Steel Shaft 5/8" Diameter, 24" Length	McMaster-Carr	2
4638K511	Zinc-Pltd STL, 1/8 Pipe Sz, Hex-Socket Plug	McMaster-Carr	4
89015K18	Multipurpose Aluminum (Alloy 6061) .125" Thick, 12" X 12"	McMaster-Carr	1
1327K113	Miniature 12L14 Drive Steel Shaft 1/4" OD, 3" Length	McMaster-Carr	2
47065T149	Double End-Feed Fastener, for 1-1/2" Aluminum Inch T-Slotted Framing System, packs of 4	McMaster-Carr	2
EM1-0-500-N	EM1 Transmissive Optical Encoder Module, 500 LPI	US Digital	1
LIN-500-21-N	LIN Transmissive Linear Strip, 500 LPI, No Index	US Digital	1

Z-Stage (per screw drive unit; 3 units total)

Part #	Part Name	Vendor	Quantity
ROB-10735	Big Easy Driver	SparkFun Electronics	3
23Y002D-LW8	NEMA 23 double-shaft stepper motor, 76 oz-in	Anaheim Automation	3
99030A005	1018 Carbon Steel Precision ACME Threaded Rod 1/2"-10 Sz, 1/10" Travel Distance/Turn, 3'L, RH Thread	McMaster-Carr	3
6208K541	Aluminum Helical Beam Clamp-on Shaft Coupling 1/2" X 1/4" Bore, 1-1/4" Length, 1-1/4" OD	McMaster-Carr	3
6061K151	Hardened Precision Steel Shaft 5/8" Diameter, 24" Length	McMaster-Carr	6
9440T41	Graphite SAE 841 Bronze Flange Bearing for 5/8" Shaft Dia, 3/4" OD, 1" Length	McMaster-Carr	3
6546K412	Multipurpose Aluminum (Alloy 6061) Rect Tube 1/8" Wall Thickness, 2" X 3", 3' Length	McMaster-Carr	3
5909K31	Cage Assembly for 1/2" Shaft Diameter, 15/16" OD Steel Thrust Needle-Roller Bearing	McMaster-Carr	6
5909K44	.032" Thick Washer for 1/2" Shaft Diameter Steel Thrust Needle-Roller Bearing	McMaster-Carr	12
94815A107	Plain Steel ACME 2G Hex Nut Right-Hand, 1/2"-10 ACME Size	McMaster-Carr	6
9712K74	High-Carbon Steel Belleville Disc Spring .505" ID, 1.000" OD, .035" Thick, packs of 12	McMaster-Carr	1
90126A033	Zinc-Plated Steel Type A SAE Flat Washer 1/2" Screw Size, 1-1/16" OD, .07"-.13" Thick, packs of 55	McMaster-Carr	1
47065T149	Double End-Feed Fastener, for 1-1/2" Aluminum Inch T-Slotted Framing System, packs of 4	McMaster-Carr	3

Enclosure

Part #	Part Name	Vendor	Quantity
47065T327	Aluminum Inch T-Slotted Framing System Drop-in Fastener W/Spring-Loaded Ball, for 1-1/2"	McMaster-Carr	216
90134A030	Spring Steel Triple-Wave Spring Washer 5/16" Screw Size, .45" OD, .01" Thick (pack of 50)	McMaster-Carr	5
91083A030	Plain Steel Type A SAE Flat Washer 5/16" Screw Size, 11/16" OD, .05"- .08" Thick (pack of 192)	McMaster-Carr	2
5537T248	Aluminum Metric T-Slotted Framing System Drop-in Fastener W/Rubber Handle, 4 mm Hex, for 40mm	McMaster-Carr	6
5190A21	Alum Load-Rated Oval Pull Hndl with Holes Black, 4-9/16" Ctr-to-Ctr, 1124# Load Rating	McMaster-Carr	4
90502A030	Plain Grade 2 Steel Extra-Wide Thin Hex Nut 5/16"-18 Thread Size, 9/16" W, 13/64" H (pack of 100)	McMaster-Carr	1
47065T212	Aluminum Inch T-Slotted Framing System Plate, Double, 4-Hole, for 1-1/2" Extrusion	McMaster-Carr	2